Dalton Transactions

Luminescent Rhenium(I) Tricarbonyl Complexes with Pyrazolylamidino Ligands: Photophysical, Electrochemical, and Computational Studies

Journal:	*Dalton Transactions*
Manuscript ID:	Draft
Article Type:	Paper
Date Submitted by the Author:	n/a

Complete List of Authors:	Gomez Iglesias, Patricia; Universidad de Valladolid, Guyon, Fabrice; Université de Franche-Comté, Khatyr, Abderrahim; Université de Franche-Comté, Institut UTINAM UMR 6213 Ulrich, Gilles; CNRS, UMR7515 Knorr, Michael; Université de Franche-Comté, Institut UTINAM Martin-Alvarez, Jose; Universidad de Valladolid, Departamento de Quimica Inorganica Miguel, Daniel; Universidad de Valladolid, IU CINQUIMA/Quimica Inorganica Villafane, Fernando; Universidad de Valladolid, Quimica Inorganica

fervilla@qi.uva.es
Teléfono: 34 983 184620

Universidad de Valladolid
Departamento de Química Física y Química Inorgánica
Dr. Fernando Villafañe

22nd July 2015

Letter to the referees

We believe that the manuscript *"Luminescent Rhenium(I) Tricarbonyl Complexes with Pyrazolylamidino Ligands: Photophysical, Electrochemical, and Computational Studies"* deserve to be published to as a Paper in *Dalton Transactions* by the following reasons:

- New neutral and cationic rhenium(I) pyrazolylamidino complexes are herein synthesized, characterized, and subjected to spectroscopic, electrochemical, and computational studies.
- Pyrazolylamidino ligands are obtained *in situ* in a one-pot reaction from the appropriate pyrazole and coordinated nitrile, so a new strategy to design new versatile rhemium(I)tricarbonyl phosphorescent complexes is described.
- All the complexes exhibit phosphorescence decays, the emission arising from a prevalently ^{3}MLCT state. TD-DFT methods provide reasonable values for emission energies, confirming the experimental values of the emission wavelengths.
- The spectroscopic, electrochemical, and computational studies include an evaluation of the effect of the substituents at the pyrazolylamidino ligand, as well as the effect of the coordination of chlorido *vs*. bromido, and their substitution by neutral acetonitrile or pyrazole ligands to yield cationic complexes.
- This opens a new way to obtain new rhemium(I)tricarbonyl phosphorescent complexes, as targeted chelating N-donor ligand with the appropriate substituents for requested applications may be easily obtained.

Yours sincerely

Fernando Villafañe

Dalton Transactions

ARTICLE

Luminescent Rhenium(I) Tricarbonyl Complexes with Pyrazolylamidino Ligands: Photophysical, Electrochemical, and Computational Studies†

Received 00th January 20xx,
Accepted 00th January 20xx

DOI: 10.1039/x0xx00000x

www.rsc.org/

Patricia Gómez-Iglesias,[a] Fabrice Guyon,[b] Abderrahim Khatyr,[b] Gilles Ulrich,[c] Michael Knorr,[b] Jose Miguel Martín-Alvarez,[a] Daniel Miguel,[a] and Fernando Villafañe[a,*]

New pyrazolylamidino complexes *fac*-[ReCl(CO)$_3$(NH=C(Me)pz*-κ^2*N,N*)] (pz*H = pyrazole, pzH; 3,5-dimethylpyrazole, dmpzH; indazole, indzH) and *fac*-[ReBr(CO)$_3$(NH=C(Ph)pz*-κ^2*N,N*)] are synthesized via base-catalyzed coupling of the appropriate nitrile with pyrazole, or by metathesis by halide abstraction with $AgBF_4$ from a bromido pyrazolylamidino complex and subsequent addition of LiCl. In order to study both the influence of the substituents present at the pyrazolylamidino ligand, and that of the "sixth" ligand in the complex, photophysical, electrochemical, and computational studies were carried out on this series and other complexes previously described by us, of general formula *fac*-[ReL(CO)$_3$(NH=C(R')pz*-κ^2*N,N*)]$^{n+}$ (L = Cl, Br; R' = Me, Ph, n = 0; or L = NCMe, dmpzH, indzH, R' = Me, n = 1). All complexes exhibit phosphorescent decays from a prevalently ^{3}MLCT excited state with quantum yields (Φ) in the range between 0.007-0.039, and long lifetimes (τ ~ 8-1900 ns). The electrochemical study reveals irreversible reduction for all complexes. The oxidation of the neutral complexes was found to be irreversible due to halido-dissociation, whereas the cationic species display a reversible process implying the ReI/ReII couple. Density functional and time-dependent density functional (TD-DFT) calculations provide a reasonable trend for the values of emission energies in line with the experimental photophysical data, supporting the ^{3}MLCT based character of the emissions.

1. Introduction

Since the first report on the photophysical properties of rhenium(I) tricarbonyl diimine complexes 40 years ago, this class of chelate compounds has been intensively studied.[1] In the meantime, an important number of luminescent *fac*-[ReX(CO)$_3$(N-N)] complexes showing rich excited-state properties associated with their long-lived triplet metal-to-ligand charge transfer (^{3}MLCT) excited state have been widely reported.[2,3] Their photophysical properties may be adequately tuned by varying the diimine ligand, the "sixth" ligand "X" (a halide or pseudo halide for neutral complexes, a neutral ligand for cationic complexes), and the solvent.[4] These properties have led to find diverse applications for this type of compounds,[5] as biomolecular agents,[6] as photocatalysts for the reduction of CO_2,[7] as light-emitting devices,[8] or as molecular sensors or photoswitches.[9]

A panoply of diimine ligands, usually derived from bipy or phen, may be found in the literature. Nonetheless, finding a straightforward, synthetically accessible way to obtain new N,N-chelating ligands is one of the remaining challenges in this field. The photophysical properties may be adjusted by choosing the appropriate ligand, but most of the ordinarily used diimine ligands usually require synthetic methods which are often difficult and tiresome. Therefore, the possibility of using *"a la carte"* and *"easy to make"* ligands would be very welcomed by the scientists working on this field. Pyrazolylamidino ligands fulfill all these requirements, since they can be readily obtained *in situ* by the coupling reaction of pyrazoles and coordinated nitriles (Scheme 1). Although reports on the synthesis of complexes containing pyrazolylamidino ligands are relatively scarce,[10,11] a wide panel of pyrazolylamidino complexes can be synthesized by using different nitriles and pyrazoles, providing the opportunity of controlling both the electronic and steric properties of the ligand. We have recently published a systematic study on the mechanism of the metal-mediated coupling of pyrazoles and nitriles.[12] This reversible intramolecular base-catalysed coupling reaction opens a broad range of synthetic possibilities to obtain new pyrazolylamidino complexes.

[a] GIR MIOMeT-IU Cinquima-Química Inorgánica, Facultad de Ciencias, Campus Miguel Delibes, Universidad de Valladolid, 47011 Valladolid, Spain.
[b] Institut UTINAM, UMR 6213, Équipe Matériaux et Surfaces Structurés, Université de Franche-Comté, 16 Route de Gray, 25030 Besançon, France.
[c] ICPEES, ECPM, UMR 7515, CNRS-Université Louis Pasteur, 25 rue Becquerel, 67087 Strasbourg, France.

† Electronic Supplementary Information (ESI) available: Figure of the crystal structure of *fac*-[ReCl(CO)$_3$(NH=C(Me)dmpz-κ^2*N,N*)], **2**; normalized emission and absorption spectra recorded in CH_2Cl_2 of complexes **2**-**6**, **8**, **10**-**12** at 298 K; cyclic voltammograms of 10 mM **5** recorded in CH_2Cl_2 solution, and of 8.6 mM [ReBr(CO)$_3$(dmpzH)$_2$] recorded in MeCN solution; tables with selected bond distances obtained in the geometry optimization of complex **1** with different functionals and basis sets, frontier molecular orbital compositions in the ground and excited states, and calculated excited energies and dominant orbital excitations from TD-DFT for all the complexes. CCDC 1414405-1414407. See DOI: 10.1039/x0xx00000x

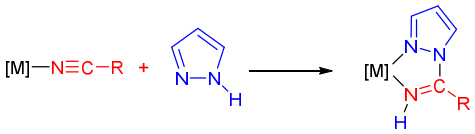

Scheme 1 Coupling reaction between a coordinated nitrile and a pyrazole to obtain a pyrazolylamidino ligand.

Since there are no previous reports dealing on photophysical studies of pyrazolylamidino complexes, we report herein the first spectroscopic, electrochemical, and computational studies on rhenium(I) tricarbonyl complexes containing pyrazolylamidino ligands.

2. Results and discussion

2.1. Synthesis and characterization

All the complexes investigated in this study are collected in Table 1. In order to study the influence of the substituents on the pyrazolylamidino ligand and of the "sixth" ligand in a given complex, a panel of complexes was synthesized, some of them previously reported by us.[11c,12] The pyrazolylamidino ligands result from the coupling of pyrazole (pzH), 3,5-dimethylpyrazole (dmpzH) or indazole (indzH) (labelled as pz-R in Table 1) with either acetonitrile or benzonitrile (NCR' in Table 1). In the neutral complexes, chlorido or bromido ligands were used, whereas acetonitrile and pyrazole (dmpzH or indzH) were coordinated in the cationic complexes (L in Table 1). This diversity allows us to discriminate the influence of different stereo electronic factors on the luminescent and electrochemical properties.

The syntheses and characterization of the species subjected to this study are described first, before discussing their properties. The syntheses of the new pyrazolylamidino complexes are presented in Scheme 2. Complexes **3**, **7**, and **8** were obtained by coupling of nitrile with pyrazole, using NaOH (aq) as catalyst, as previously reported by us.[12] Chlorido complexes **1** and **2** were instead obtained from the previously synthesized bromido pyrazolylamidino complexes by abstracting the bromido ligand with $AgBF_4$ and subsequent addition of chloride. Alternatively, complexes **1** and **2** can also be obtained by the same manner as complex **3**, that is by coupling of the corresponding nitrile with pyrazole. However, in these cases the yields are much lower using this route, as these processes usually reach an equilibrium between the mixed nitrile-pyrazole and the final pyrazolylamidino complexes,[12] and this equilibrium is driven to the starting mixture for chlorido complexes **1**-**3**, whereas for bromido complexes **4**-**8** it is driven to the final pyrazolylamidino complexes.

The spectroscopic and analytical data support the proposed geometries and are collected in the Experimental Section. The hydrogen atoms in *ortho* position of the phenyl substituents in benzonitrile-derived complexes **7** and **8** display broad signals in the ^{1}H NMR spectra at room temperature, probably due to the slowing down of the phenyl group rotation. Spectra recorded at lower temperatures gave the expected pattern (see Experimental Section). Furthermore, complexes **1** (Figure 1), **2** (Figure S1), and **7** (Figure 2) were characterized by single-crystal X-ray diffraction studies. The distances and angles (CCDC 1414405-1414407) are similar to those found in other pyrazolylamidinorhenium complexes.[11,12] In complexes **2** and **7**, the *N*-bound hydrogens of the pyrazolylamidino ligands are involved in hydrogen bonding with a chlorido ligand of an adjacent molecule, or with the oxygen atom of a THF molecule present in the crystal, respectively. The distances and angles detected (H(3)···Cl(1) 2.279(8) Å, N(3)···Cl(1) 3.267(8) Å, N(3)–H(3)···Cl(1) 160.2(4)°, for **2**, and H(3)···O(91), 1.815(8) Å; N(3)···O(91) 2.837(8) Å, N(4)–H(3)···O(91) 171.8(4)°) for **7** may be considered respectively as "weak" and "moderate" hydrogen bonds.[13]

Table 1 Pyrazolylamidino complexes used in this study.

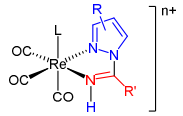

Compd.	n	L	pz-R	R'	ref.
1	0	Cl	pz	Me	this work
2	0	Cl	dmpz	Me	this work
3	0	Cl	indz	Me	this work
4	0	Br	pz	Me	11c
5	0	Br	dmpz	Me	11c
6	0	Br	indz	Me	12
7	0	Br	dmpz	Ph	this work
8	0	Br	indz	Ph	this work
9	1 (ClO_4^- salt)	NCMe	dmpz	Me	11c
10	1 (ClO_4^- salt)	NCMe	indz	Me	12
11	1 (ClO_4^- salt)	dmpzH	dmpz	Me	11c
12	1 (ClO_4^- salt)	indzH	indz	Me	12

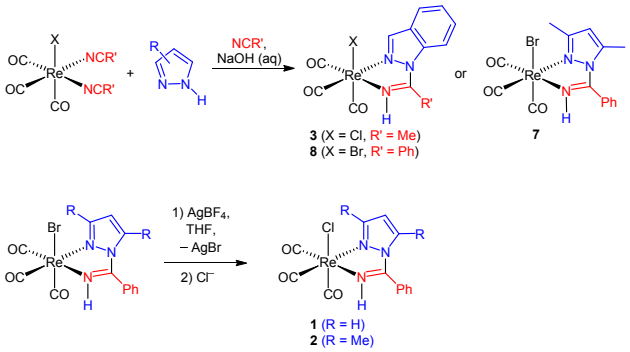

Scheme 2 Syntheses of the new pyrazolylamidino complexes.

2.2. Photophysical Studies

One main objective of this work was investigating the photophysical properties of our family of rhenium(I) tricarbonyl complexes containing pyrazolylamidino ligands, as there are not previous reports on the photophysical properties of complexes bearing these ligands. The absorption and emission spectral data collected for all complexes are

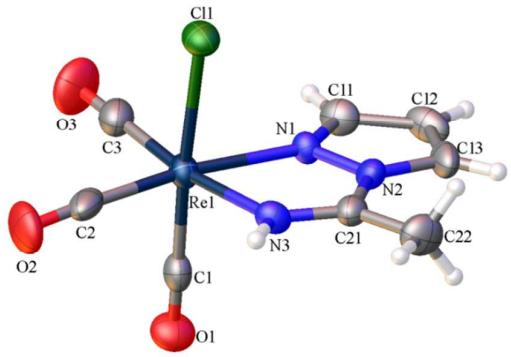

Fig. 1 Perspective view of *fac*-[ReCl(CO)$_3$(NH=C(Me)pz-κ^2*N,N*)], **1,** showing the atom numbering. Thermal ellipsoids are drawn at 50% probability. Selected bond lengths (Å) and angles (deg): N1-Re1 2.164(6), N1-N2 1.365(11), C21-N2 1.399(13), C21-N3 1.289(12), N3-Re1 2.158(8), Cl1-Re1 2.500(2); C1-Re1-Cl1 176.8(2), C1-Re1-N1 89.9(3), C1-Re1-N3 95.0(4), C2-Re1-Cl1 95.0(3), C2-Re1-N1 170.7(4), C2-Re1-N3 97.8(4), C3-Re1-Cl1 91.5(4), C3-Re1-N1 99.6(4), C3-Re1-N3 171.4(4), N1-Re1-Cl1 87.0(2), N3-Re1-Cl1 83.3(2), N3-Re1-N1 73.3(3), N2-N1-Re1 114.4(5), N1-N2-C21 118.1(7), N3-C21-N2 114.7(8).

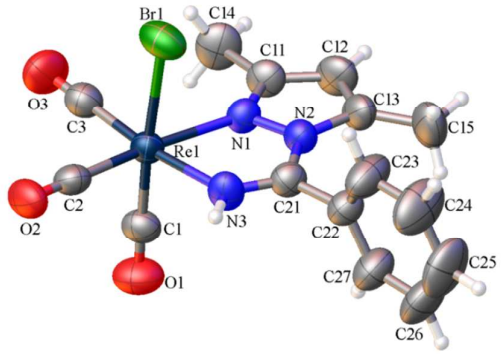

Fig. 2 Perspective view of *fac*-[ReBr(CO)$_3$(NH=C(Ph)dmpz-κ^2*N,N*)], **7**, showing the atom numbering. Thermal ellipsoids are drawn at 50% probability. Selected bond lengths (Å) and angles (deg): Re1-N1 2.169(4), N1-N2 1.385(6), N2-C21 1.411(7), N3-C21 1.266(7), Re1-N3 2.130(5), Re1-Br1 2.6274(7); N1-Re1-Br1 84.02(12), N3-Re1-Br1 84.97(13), N3-Re1-N1 72.98(17), C1-Re1-Br1 176.81(19), C1-Re1-N1 93.8(2), C1-Re1-N3 92.2(2), C2-Re1-Br1 92.49(17), C2-Re1-N1 169.9(2), C2-Re1-N3 97.3(2), C3-Re1-Br1 91.15(19), C3-Re1-N1 100.9(2), C3-Re1-N3 173.0(2), N2-N1-Re1 114.4(3), N1-N2-C21 116.1(4), N3-C21-N2 115.0(5), C21 N3 Re1 121.3(4).

summarized in Table 2. The electronic absorption and emission spectra of complexes **1** to **12** have been measured at 298 K using CH_2Cl_2 as solvent. Figure 3 shows representative absorption and emission spectra of neutral chlorido complex **1** and of the cationic complex **9**, respectively. The absorption spectra of all complexes (see ESI, Figure S2) exhibit high-energy transitions with maxima between 230 and 300 nm, and a tail reaching up to 480 nm. The absorption data of the complexes are qualitatively similar to related Re(I) compounds already published.[2a,14] Selected examples displaying similar absorption spectra are *fac*-[ReX(CO)$_3$(N-N)] where X = Cl or Br, and N-N represents a bidentate *N*-heterocyclic carbene,[15] or pyridyl-triazole derivatives[16] possessing imine-type *N*-donor sites. Therefore it seems justified to interpret the absorption features of our rhenium(I) complexes in an analogous manner. As described below, the results of the computational study also support this assignment. Intense bands due to an intraligand (IL) origin are observed in the UV region at high energy (230-300 nm). The lowest energy absorption bands listed in Table 2 are assigned to a mixture of MLCT Re→π*(L), ligand-to-ligand charge-transfer (LLCT), and halide-to-ligand charge-transfer (XLCT) transitions. The XLCT character is supported by the fact that the absorption maxima shifts to lower energy upon changing the halide ligands from Cl to Br, because the oxidation of the metal becomes progressively easier upon decreasing the electronegativity of the halide. The same behaviour was also observed for the series [Re$_2$(μ-X)$_2$(CO)$_6${μ-(1,2-diazine)}] when changing the nature of the halide (X = Cl, Br, I).[17]

In order to evaluate the halide influence on the photophysical properties, the series of chlorido complexes (**1**-**3**) is compared with their bromido-substituted analogous (**4**-**6**). After excitation at 390 nm, the comparison of the emission bands reveals that those of chlorido complexes **1**, **2** and **3** show a slight hypsochromic shift with respect to their bromido counterparts **4**, **5** and **6**. As reported by Bertrand *et al*.,[16] these profiles are typical of the emission from MLCT/XLCT excited states when considering band shapes and the values of the emission wavelengths.

The luminescence quantum yields Ø of the pyrazolylamidino complexes were determined using cresyl violet as a luminescence quantum yield standard,[18] all measurements have been performed in deaerated solvents. The quantum yields of our complexes are relatively weak, independently of the halide or counter ion, and fall in the range reported for other "*fac*-Re(CO)$_3$" complexes.[15,19] Nevertheless, in the case of the halide series **1**-**6**, somewhat higher quantum yields are found for the bromido-derivatives **4**-**6** (Ø 0.017-0.026 %) compared to those of chlorido-derivatives **1**-**3** (Ø 0.015-0.022 %). Although complexes **4** and **5** emit at lower excited energy states, thus contradicting trends dictated by the energy gap law (EGL),[20] the shorter lifetime values for complexes **1**, **2**, **3** and **6** might be caused by competing photochemical pathways triggered upon excitation. Despite a long-lived emission due to a ^{3}MLCT transition of pz-complex **4** (890 ns), with τ twice than that of the dmpz complex **5** (430 ns), the quantum yields of both compounds are quite close, around 0.02-0.03%.

The following trends are noticed: (i) introduction of electron-donating groups in the pirazole core causes a weak shift to lower λ_{em}. This effect can be observed when comparing pyrazole complexes **1** and **4** with 3,5-dimethylpyrazole complexes **2** and **5**, resulting in $\Delta\lambda_{em}$ ~ [13 nm/409 cm^{-1}] and [8 nm/248 cm^{-1}] respectively. (ii) When the "sixth" ligand is replaced from an anionic σ-donor/π-donor ligand (chlorido in complexes **2**, **3**, and bromido in complexes **5**, **6**) by a neutral σ-donor ligand (acetonitrile in complexes **9**, **10**) there is an hypsochromic shift in the emission that ranges from $\Delta\lambda_{em}$ = [33 nm/1130 cm^{-1}] when comparing complexes **2**

and **9**, to $\Delta\lambda_{em}$ = [49 nm/1585 cm^{-1}] when comparing complexes **6** and **10**. A simultaneous enhancement of the non-radiative constant is observed, which may be induced by the change of the σ-donor/π-donor character of chlorido/bromido by the σ-donor character of acetonitrile in the complex, thus favouring a non-emissive vibrational de-excitation pathway. This is reflected by a strong drop of the lifetime τ from 430 to 17 ns. (iii) The replacement of the imine-methyl group in bromido complex **6** by a phenyl group in indz-complex **8** induces a red-shift of the emission with $\Delta\lambda_{em}$ ~ [25 nm/710 cm^{-1}], concomitantly with an enhanced non-radiative constant.

Table 2 Absorption and emission data of complexes **1** to **12** in CH_2Cl_2 at 298 K.*

Comp	Absorption	Emission				
	λ nm (ε x 10^{-3} $M^{-1}cm^{-1}$)	λ_{em} (nm) [λ_{excit} = 390 nm]	Ø x 10^{-3} (± 8%)	τ (ns)	k_r 10^4 s^{-1}	k_{nr} 10^6 s^{-1}
1	264 sh (13), 360 (7)	570	15	220	6.8	4.5
2	232 (16.7), 261 sh (10.9), 352 (5)	557	22	254	8.6	3.85
3	260 (15.1), 304 (5), 316 (5), 367 (6.7)	559	18	210	8.6	4.7
4	246 (17.1), 267 sh (15.8), 368 (2)	572	17	890	1.9	1.1
5	248 (17.4), 283 (20.2), 356 (21.3)	564	26	430	6.0	2.3
6	251 (20.1), 269 sh (18.9), 379 (3.8)	581	21	180	11.7	5.4
8	233 (19.1), 273 (19.4), 310 sh (4.2),323 sh (3.3), 381 (3.7)	606	11	35	31.4	28.3
9	233 (19.5), 254 (20.2), 324 (10.3)	524	12	17	7.1	58.1
10	246 (21.1), 313 (8.4), 340 (8.5)	532	16	8	200	123
11	260 (10.2), 346 (16)	536	7	560	1.25	1.77
12	254 (21.7), 282 (24.1), 359 (13.7)	544	39	1900	2.1	0.5

* Not reliable spectra could be obtained for **7** due to its instability in CH_2Cl_2 solution.

This same effect is also noticed when comparing the emission maxima of complex **6** with those of **12** ($\Delta\lambda_{em}$ ~ [17 nm/1170 cm^{-1}]) and **10** ($\Delta\lambda_{em}$ ~ [49 nm/1585 cm^{-1}]). Note that a considerable diminution of the non-radiative constant, evidenced by a longer emission lifetime, is observed when the indazole ligand in **12** is replaced by an acetonitrile ligand in **10**. A similar long life-time emission at 536 nm is observed for cationic complex **11**, where the Re centre is coordinated by a chelating pyrazolylamidino ligand containing a dmpz fragment, and a *N*-bound 3,5-dimethylpyrazole ligand. The emitting level can be assigned as ^{3}MLCT transition according to usual consideration of the position and shape of the emission band for complexes **9** to **12**. This interpretation is consistent with those previously reported for similar carbonyl and diimine ligand coordinated to a Re(I) d^6 low-spin centre assigned as ^{3}MLCT emitters,[21] and with the results of the theoretical calculations carried out on this complexes (see below).

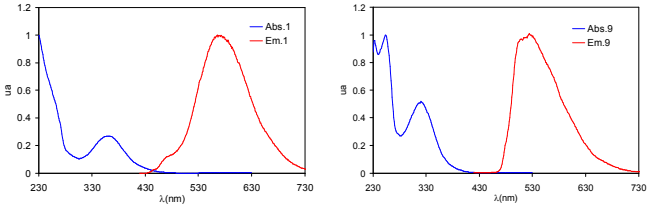

Fig. 3 Emission (red) and absorption (blue) spectra recorded in CH_2Cl_2 of complexes **1** (left) and **9** (right) at 298 K.

In summary, the substitution of chloride in complexes **1**-**3** by bromide (complexes **4**-**6**) is translated by a small hypsochromic shift. The same behaviour is observed when the hydrogens at the 3- and 5- positions of the pyrazole core (in **4**) are substituted by two electron-donating methyl groups (in **5**). The substitution of the bromido ligand in dmpz complex **5** by acetonitrile (in **9**) gives rise to an increase of the energy of the emitter level by 1354 cm^{-1}. The replacement of the methyl group at the amidino fragment (in **6**) by a phenyl group (in **8**) induces a red-shift of the emission by 710 cm^{-1}. All the complexes exhibit phosphorescent decays from the ^{3}MLCT excited state, and their quantum yields (Φ ~ 0.007-0.039) correspond to those reported previously for other rhenium(I) tricarbonyl complexes. Their long lifetimes (τ ~ 8-1900 ns), are a further proof that the emissions arise from a prevalently ^{3}MLCT state.

2.3. Electrochemical Study

The redox properties of each compound have been investigated by cyclic voltammetry in MeCN solution in the potential region from −2.30 V to 1.50 V. Scans rates between 0.025 and 2.5 V s^{-1} were examined. Cyclic voltammograms have also been recorded for some samples in CH_2Cl_2 in order to probe the influence of a non-coordinating solvent on their redox properties. Table 3 lists the measured redox potentials in MeCN.

All compounds display an irreversible cathodic wave between −1.47 V and −2.25 V.‡ Due to the significant shift of the cathodic peak potential (E^p_{red}) when changing the nature of the pyrazolylamidino ligand, a pyrazolylamidino-based reduction is assigned to this wave. This is supported by the results of the computational study (see below), since the LUMO has mainly an amidino contribution. For the neutral complexes, the irreversibility of the process is attributed to the halide dissociation, as reported for related compounds.[22] This is corroborated by the observation of an anodic wave at *ca.* +0.5 V for the bromido complexes **4**-**8**, which may result from the oxidation of bromide when the scan starts towards reduction before oxidation potentials (see curves corresponding to the 2nd and 3rd scans of **5** in figure 4).

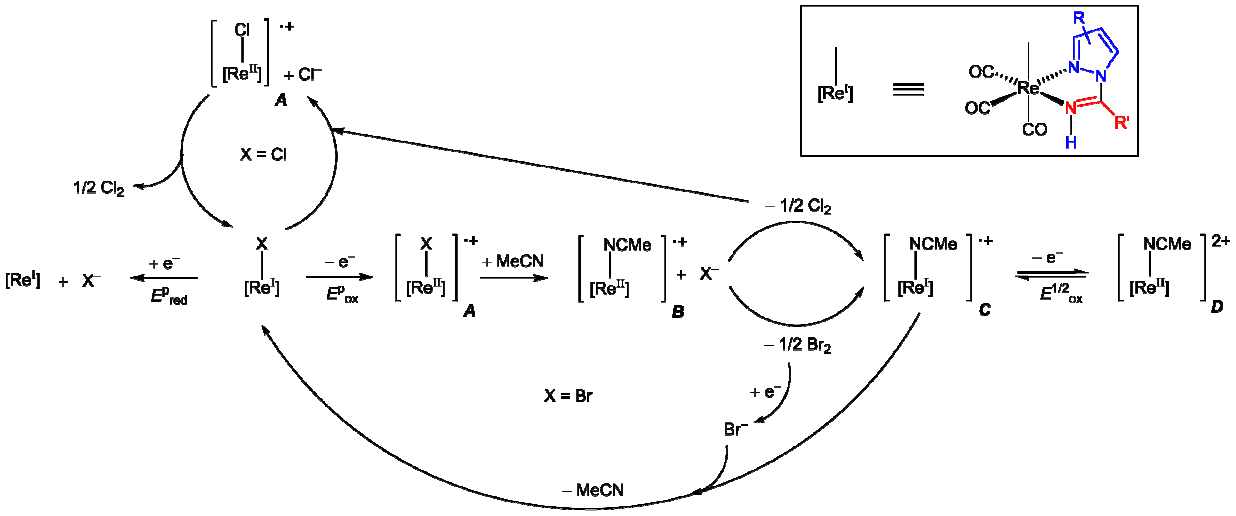

Scheme 3 Electrochemical processes proposed for the pyrazolylamidino complexes.

Neutral complexes (**1**-**8**) exhibit two oxidation processes (see Figure 4 for **5**). An irreversible peak is observed, even for a scan rate of 2.5 V s^{-1}, at 0.90 ± 0.02 V, followed by an electrochemically reversible one at 1.32 ± 0.02 V. In contrast, the cationic species (**9**-**12**) display only one quasi-reversible wave in the range 1.15-1.34 V (see Figure 4 for **9**). For compounds **9**-**11**, the ratio of peak currents (i_{pa}/i_{pc}) is equal to 1 at a scan rate of 100 m V s^{-1}, whereas the reversibility is observed only for scan rates above 500 mV s^{-1} for compound **12**. For the bromido complexes **4**-**8** the oxidation peak at 0.90 V is coupled in the following scan to a reduction peak at *ca*. 0.55 V (see Figure 4 for **5**). In all, the cyclic voltammograms of the neutral compounds investigated here are comparable to that of *fac*-[ReCl(CO)$_3$(dmbipy)] (dmbipy = 4,4'-dimethyl-2,2'-bipyridil).[23] In this case the first oxidation was found to produce chlorine and *fac*-[Re(MeCN)(CO)$_3$(dmbipy)]$^+$. We propose a similar EC mechanism for pyrazolylamidino halido complexes **1**-**8** in a first stage (Scheme 3). The potentials E^p_{ox} are independent of the nature of the ligands (Table 3), and therefore the process is assigned to a metal centred oxidation, leading to the formally 17-electron monocationic species *fac*-[Re^{II}X(CO)$_3$(NH=C(R')pz*-κ^2*N,N*)]$^{\bullet+}$, ***A***. This is followed by dissociation of the halide with concomitant coordination of a molecule of MeCN to give 17-electron cationic species *fac*-[Re^{II}(NCMe)(CO)$_3$(NH=C(R')pz*-κ^2*N,N*)]$^{\bullet+}$, ***B***. This Re^{II} adduct is reduced by reaction with halide to give X_2 and the 18-electron cation *fac*-[Re^{I}(NCMe)(CO)$_3$(NH=C(R')pz*-κ^2*N,N*)]$^{\bullet+}$, ***C***, which is electrochemically reversibly oxidized at 1.32 ± 0.02 V, to give *fac*-[Re^{II}(NCMe)(CO)$_3$(NH=C(R')pz*-κ^2*N,N*)]$^{2+}$, ***D*** (Scheme 3). The very close half-wave potentials of dmpz complexes **2**, **5** and **9** on the one hand, and of the indz complexes **6** and **10** on the other hand,[§] (Table 3 and Figure 4) support this proposal. Moreover, the wave observed at 1.32 ± 0.02 V is irreversible when the cyclic voltammograms of the halido complexes are performed in CH_2Cl_2 (Figure S3), as expected for the oxidation of *fac*-[Re(CO)$_3$(NH=C(R')pz*-κ^2*N,N*)]$^{\bullet+}$, which would lead to a very unstable 15 electron species. The relatively limited deviation between all the half-wave potentials collected ($E^{1/2}_{ox}$ in Table 3) pleads for an electronic transfer implying the Re(I)/Re(II) couple, as indicated in Scheme 3.

The cathodic wave observed at 0.55 V for the bromido complexes **4**-**8** is assigned to the reduction of molecular bromine to bromide,[24] which reacts with *fac*-[Re^{II}(NCMe)(CO)$_3$(NH=C(R')pz*-κ^2*N,N*)]$^{\bullet+}$, ***C***, to regenerate the starting materials (Scheme 3). Thus, any wave due to oxidation of the bromine is observed when scan is cyclized between −0.3 to +1.5 V at a scan rate of 100 mV s^{-1}.

In the cyclic voltammograms of the chlorido complexes **1**-**3**, the reduction of chlorine is not detected. Chlorine is a stronger oxidizing agent than bromine, and therefore should oxidize the starting complexes **1**-**3** (Scheme 3).

Table 3. Redox potentials of the pyrazolylamidino complexes.

Compd.	E^p_{red}	E^p_{ox}	$E^{1/2}_{ox}$
1	−2.08	+ 0.92	+ 1.34
2	−2.25	+ 0.89	+ 1.30
3	−1.30	+ 0.93	[a]
4	−2.10	+ 0.91	+ 1.34
5	−2.20	+ 0.88	+ 1.31
6	−1.47	+ 0.91	+ 1.32
7	−1.87 and −2.14	+ 0.91	+ 1.33
8	−1.84	+ 0.92	+ 1.34
9	−1.96		+ 1.32
10	−1.80		+ 1.34
11	−1.96		+ 1.15
12	−2.04		+ 1.32

[a] The low solubility of **3** in MeCN precluded a clear determination of $E^{1/2}_{ox}$.

The irreversibility of the oxidation herein observed for the neutral pyrazolylamidino complexes is not a general feature for neutral rhenium(I) tricarbonyl diimine complexes. For example, *fac*-[ReX(CO)$_3$(^{t}Bu-DAB)] (X = Cl or Br; ^{t}Bu-DAB = 1,4-di-tert-butyl-1,4-diazabutadiene) exhibits a reversible oxidation at a potential similar to those listed as E^p_{ox} in Table 3.[25] In order to assess the influence of the pyrazolylamidino ligands in the redox properties of these *fac*-[ReX(CO)$_3$(diimine)] complexes, this study was completed by the characterization of the electrochemical behaviour of *fac*-[ReBr(CO)$_3$(dmpzH)$_2$][26] and *fac*-[ReBr(CO)$_3$(MeCN)(dmpzH)][11c] complexes. *fac*-[ReBr(CO)$_3$(dmpzH)$_2$] exhibits a reversible wave at 0.93 V (Figure S4), whereas for *fac*-[ReBr(CO)$_3$(MeCN)(dmpzH)] the ratio i_{pa}/i_{pc} centred at 0.99 V is equal to 0.4 at a scan rate of 100 mV s^{-1}. It is noteworthy that in both cases reduction of bromine is not detected in the following scan. Thus, the stabilities of *fac*-[Re^{II}Br(CO)$_3$(dmpzH)$_2$]$^{\bullet+}$ and *fac*-[Re^{II}Br(CO)$_3$(MeCN)(dmpzH)]$^{\bullet+}$ contrast with that of *fac*-[Re^{II}Br(CO)$_3$(pyrazolylamidino)]$^{\bullet+}$, what may be interpreted considering the difference of lability of the Re-Br bond in these compounds.

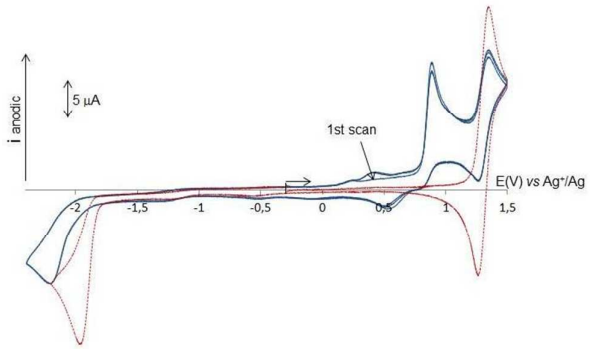

Fig. 4. Cyclic voltammograms recorded in MeCN solutions of 15 mM **5** (blue, 3 scans) and 16 mM **9** (red, 1 scan). Scan rate: 100 mV/s. Initial potential: –0.3 V .

2.4. Computational Study

All the complexes were also studied theoretically by means of density functional and time-dependent density functional (TD-DFT) calculations. Computational details can be found in the Experimental Section, the relevant types of complexes are discussed here, and the complete list of results is included in the ESI. The ground-state geometry was optimized at the PBE1PBE level (PBE0) with no symmetry restraints for all the complexes and the minimum obtained compares well with the structure obtained by X-ray diffraction when available (see Tables S1 and S2 in the ESI).

The partial frontier molecular orbital compositions and energy levels of compounds **1** and **9**, as models for neutral (**1**-**8**) and cationic (**9**-**12**) complexes are listed in Tables 4 and 5, respectively.

It can be seen that the highest occupied molecular orbitals (HOMOs) have a mixed Re/CO/Cl character with different contributions in the case of the neutral complex **1**, while for

Table 4 Frontier Molecular Orbital Compositions (%) in the Ground State for Complex **1** at the PBE1PBE Level (L = amidino).

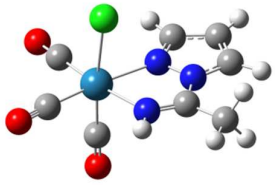

		Contribution (%)				
Orbital	**E (eV):**	**Re:**	**Cl:**	**CO:**	**L:**	**main bond type**
HOMO-4	–7.76	12.29	55.89	3.97	27.85	d(Re) + p(Cl) + π(L)
HOMO-3	–7.66	9.84	58.90	3.35	27.91	d(Re) + p(Cl) + π(L)
HOMO-2	–6.98	68.90	0.53	28.57	2.00	d(Re) + π(CO)
HOMO-1	–6.40	46.90	25.98	20.78	6.33	d(Re) + p(Cl) + π(CO)
HOMO	–6.32	47.08	25.77	22.84	4.32	d(Re) + p(Cl) + π(CO)
LUMO	–2.04	4.60	1.68	5.82	87.91	π*(L)
LUMO+1	–0.55	29.29	1.08	65.50	4.14	p(Re) + π*(CO)
LUMO+2	–0.31	27.97	2.90	61.25	7.89	p(Re) + π*(CO)

Table 5 Frontier Molecular Orbital Compositions (%) in the Ground State for Complex **9** at the PBE1PBE Level (L = amidino).

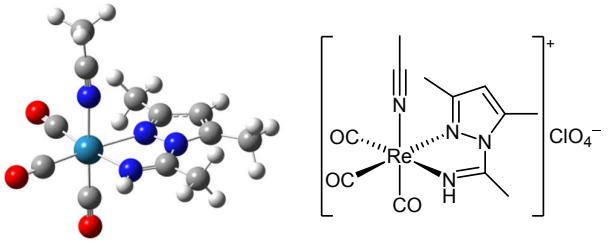

		Contribution (%)				
Orbital	**E (eV):**	**Re:**	**MeCN:**	**CO:**	**L:**	**main bond type**
HOMO-3	–8.39	6.21	1.44	2.11	90.25	π(L)
HOMO-2	–7.5	69.58	0	27.9	2.52	d(Re) + π(CO)
HOMO-1	–7.17	59.02	4.74	23.04	13.21	d(Re) + π(CO) + π(L)
HOMO	–7.11	54	4.09	21.28	20.63	d(Re) + π(CO) + π(L)
LUMO	–2.37	5.65	0.5	7.38	86.48	π*(L)
LUMO+1	–1.27	26.08	18.09	51.59	4.23	p(Re) + π*(CO) + π*(MeCN)
LUMO+2	–0.93	19.19	25.13	51.32	4.36	p(Re) + π*(CO) + π*(MeCN)

the cationic complex **9** there is also a non negligible contribution from the pyrazolylamidino ligand. In both cases the LUMO is mainly centred in the amidino ligand.

The calculated absorption energies associated with their oscillator strengths, the main configuration and their assignments, together with the experimental results for complexes **1** and **9** are given in Tables 6 and 7, respectively.

For the neutral complex **1**, the low lying absorption measured experimentally at 360 nm can be assigned to the singlet excited state S_2 (366 nm), which consists primarily in the excitation from HOMO-1 with d(Re) + p(Cl) + π(CO) main bond type to LUMO with π*(amidino) main bond type. Thus, this transition has a MLCT/LLCT/XLCT character, consistent with the trends experimentally observed for the absorption maxima shifts, already discussed in the photophysical study section above.

On the other hand, when the halide ligand is replaced by a neutral ligand (acetonitrile or a pyrazole) to obtain a cationic complex, the lowest experimental absorption is blue-shifted (found at 324 nm in complex **9** with respect to 352 nm in the chlorido-dmpz neutral complex **2**). The calculated singlet excited state (S_2 also in this case) consists now of two transitions, from HOMO-1 and HOMO to LUMO, which contribute almost equally. The composition of HOMO-1 and HOMO orbitals has a significant contribution from the amidino moiety, 13 and 21% respectively, and therefore, the transition has a less marked charge transfer character than in the case of the neutral complexes. The MLCT transition plays an important role in the excitation and, consequently, the absorption intensity of **9** is stronger than **1**, as observed experimentally.

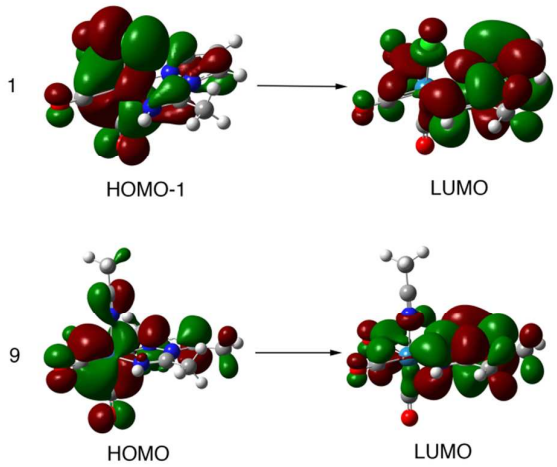

Fig. 5 Single electron transitions for the low lying absorptions of complexes **1** and **9**, calculated at the TD-DFT/PBE0 level.

Moreover, the weaker π-donating ability of acetonitrile with respect to the halido ligand, makes the HOMO and HOMO-1 orbitals less energetic, what is consistent with the blue-shift observed in the absorption.

The MLCT character of the low lying absorption transitions for complexes **1** and **9** can be observed in Figure 5, where the relevant molecular orbitals are depicted for both compounds.

The lowest triplet states T_1 of all the complexes have been optimized by the UPBE0 method and, from the geometry thus obtained, the TD-DFT method has been applied to calculate their phosphorescence emission. The composition of the

Table 6 Calculated Excited Energies, Dominant Orbital Excitations, and Oscillator Strength (*f*) from TD-DFT Calculations for Complex **1**.

state	excitation	Coef.	E_{calc} (eV)	λ_{calc} (nm)	*f*	λ_{exp} (nm)	Character
S_1	HOMO → LUMO	0.70	3.21	386	0.0035		MLCT/LLCT/XLCT
S_2	HOMO-1 → LUMO	0.69	3.39	366	0.0964	360	MLCT/LLCT/XLCT
S_8	HOMO-4 → LUMO	0.64	4.76	261	0.1178	264	MLCT/XLCT/ILCT
	HOMO-3 → LUMO	0.27					

Table 7 Calculated Excited Energies, Dominant Orbital Excitations, and Oscillator Strength (*f*) from TD-DFT Calculations for Complex **9**.

state	excitation	Coef.	E_{calc} (eV)	λ_{calc} (nm)	*f*	λ_{exp} (nm)	Character
S_1	HOMO-1 → LUMO	0.46	3.70	355	0.0133		MLCT/LLCT/ILCT
	HOMO → LUMO	0.53					
S_2	HOMO-1 → LUMO	0.52	3.86	321	0.1784	324	MLCT/LLCT/ILCT
	HOMO → LUMO	0.45					
S_8	HOMO-2 → LUMO+2	0.40	4.97	250	0.0561	254	MLCT/LLCT/ILCT
	HOMO → LUMO+2	0.40					/LXCT
S_9	HOMO-3 → LUMO	0.67	5.12	242	0.1457	233	ILCT

Table 8 Molecular Orbital Compositions in the Excited States.

			Contribution (%)			
Complex	**Orbital**	**Energy (eV):**	**Re:**	**"sixth" ligand:**	**CO:**	**amidino:**
1	HOMO	–5.87	46.33	18.86	17.50	17.31
	LUMO	–2.37	5.66	2.43	8.96	82.95
9	HOMO	–6.61	47.79	3.87	18.38	29.97
	LUMO	–2.78	5.19	0.61	7.48	86.72

Table 9 Calculated Emission Energies and Dominant Orbital Emissions from TD-DFT Calculations.

Complex	state	Transition	Coef.	E_{calc} (eV)	λ_{calc} (nm)	λ_{exp} (nm)	Character
1	T_1	LUMO → HOMO	0.69	1.88	659	570	^{3}MLCT/^{3}LLCT/^{3}XLCT
9	T_1	LUMO → HOMO	0.67	2.07	599	524	^{3}MLCT/^{3}LLCT/^{3}ILCT

HOMO and LUMO orbitals is very similar to those of the singlet ground state, as can be seen by inspection of the values gathered in Table 7. Therefore, the character of the emissions is ^{3}MLCT/^{3}LLCT/^{3}XLCT for the neutral complexes and ^{3}MLCT/^{3}LLCT/^{3}ILCT for the cationic complexes, and the calculated emission energies and the corresponding transition characters for both types of complexes are shown in Table 9.

Although the TD-DFT computing methods cannot exactly reproduce the experimental values of the emission wavelengths, it can provide reasonable values that follow the same trend. In this respect, the substitution of the halide in the neutral complexes by a weaker π-donor stabilizes the HOMO, makes wider the HOMO-LUMO energy gap and, as in the absorption transitions, a blue-shift in the wavelength is observed.

3. Experimental Section

3.1. General Remarks

All manipulations were performed under N_2 atmosphere following conventional Schlenk techniques. Solvents were purified according to standard procedures.[27] *fac*-[ReCl(CO)$_3$(NCMe)$_2$],[28] *fac*-[ReBr(CO)$_3$(NCMe)$_2$],[19] *fac*-[ReBr(CO)$_3$(NH=C(Me)pz-κ^2*N,N*)],[11c] *fac*-[ReBr(CO)$_3$(NH=C(Me)dmpz-κ^2*N,N*)],[11c] and *fac*-[ReBr(CO)$_3$(NH=C(Me)indz-κ^2*N,N*)],[12] were obtained as previously described. Table 1 collects references for the preparation and characterization of some of the complexes herein studied. All other reagents were obtained from the usual commercial suppliers, and used as received. Infrared spectra were recorded in a Perkin-Elmer FT-IR spectrum BX apparatus using 0.2 mm CaF_2 cells for solutions or KBr pellets for solid samples. NMR spectra were recorded in Varian MR500 instrument at room temperature (r.t.) unless otherwise indicated, and are referred to the internal residual solvent peak for ^{1}H and ^{13}C{^{1}H} NMR. Assignment of the ^{13}C{^{1}H} NMR data was supported by 2D heteronuclear experiments and relative intensities of the resonance signals. Elemental analyses were performed on a Perkin-Elmer 2400B microanalyzer.

3.2. *fac*-[ReCl(CO)$_3$(NH=C(Me)pz-κ^2*N,N*)], 1.

fac-[ReBr(CO)$_3$(NH=C(Me)pz-κ^2*N,N*)] (0.138 g, 0.3 mmol) and $AgBF_4$ (0.068 g, 0.35 mmol) were stirred in THF (25 mL) for 1 h at 40 °C. The solvent was removed *in vacuo*, the complex was extracted with CH_2Cl_2 (40 mL), filtered, and the solvent was removed *in vacuo*. The pale yellow residue was then dissolved in acetone (20 mL) and LiCl (0.063 g, 1.5 mmol) was added. The mixture was stirred at r.t. overnight. The solvent was removed *in vacuo*, and the complex was extracted with THF (20 mL), filtered, and the yellow residue was crystallized in THF/hexane at −20 °C, giving a yellow microcrystalline solid, which was decanted, washed with hexane (3 × 3 mL, approximately), and dried *in vacuo*, yielding 0.111 g (89 %). IR (THF, cm^{-1}): 2021 vs, 1919 vs, 1891 vs. IR (KBr, cm^{-1}): 3175 m, 3138 m, 2025 vs, 1919 vs, 1893 vs, 1653 m, 1560 w, 1524 w, 1431 w, 1409 m, 1398 w, 1376 w, 1328 w, 1241 m, 1129 w, 1073 w, 1053 w, 1043 w, 1000 w, 961 w, 873 w, 775 m, 684 w, 630 w, 562 w, 517 w, 496 w, 472 w. ^{1}H NMR (500 MHz, Me$_2$CO-d_6): 2.96 (s, CH_3, 3 H), 6.85 (dd, *J* = 3.0 and 2.0 Hz, H^4, 1 H), 8.34 (d, *J* = 2.0 Hz, $H^{3,5}$, 1 H), 8.66 (d, *J* = 3.0 Hz, $H^{5,3}$, 1 H), 11.21 (br s, N*H*, 1 H). ^{13}C{^{1}H} NMR (126 MHz, Me$_2$CO-d_6): 19.0 (s, NC*C*H$_3$), 112.3 (s, C^4H pz), 134.1 (s, $C^{5,3}$ pz), 147.4 (s, $C^{3,5}$ pz), 164.1 (s, NH=*C*CH$_3$), 189.5 (s, *C*O), 197.9 (s, *C*O), 198.1 (s, *C*O). Anal. Calcd. For $C_8H_7ClN_3O_3Re$ C, 23.13; H, 1.70; N, 10.12. Found: C, 23. 40; H, 1.66; N, 9.98.

3.3. *fac*-[ReCl(CO)$_3$(NH=C(Me)dmpz-κ^2*N,N*)], 2.

The same procedure as for **1**, using *fac*-[ReBr(CO)$_3$(NH=C(Me)dmpz-κ^2*N,N*)] (0.170 g, 0.35 mmol) as starting material, gave 0.140 g (92 %) of **2** as a pale yellow microcrystalline solid. IR (THF, cm^{-1}): 2018 vs, 1915 vs, 1887 vs. IR (KBr, cm^{-1}): 3154 m, 3103 m, 2017 vs, 1923 vs, 1896 vs, 1882 vs, 1648 m, 1567 w, 1449 w, 1407 m, 1356 m, 1256 m, 1131 w, 1100 w, 1046 w, 895 w, 841 w, 645 w, 627 w, 516 w, 494 w, 478 w. ^{1}H NMR (500 MHz, Me$_2$CO-d_6): 2.51 (s, CH_3 dmpz, 3 H), 2.76 (s, CH_3 dmpz, 3 H), 2.97 (s, NH=CCH_3, 3 H), 6.46 (s, H^4 dmpz, 1 H), 10.82 (br s, N*H*, 1 H). ^{13}C{^{1}H} NMR (126 MHz, Me$_2$CO-d_6): 14.3 (s, *C*H$_3$ dmpz), 16.1 (s, *C*H$_3$ dmpz), 21.5 (s, N=C*C*H$_3$), 113.8 (s, C^4H dmpz), 146.8 (s, *C*CH$_3$ dmpz), 156.5 (s, *C*CH$_3$ dmpz), 165.4 (s, NH=*C*CH$_3$), 189.6 (s, *C*O), 198.4 (s, *C*O), 198.9 (s, *C*O). Anal. Calcd. For $C_{10}H_{11}ClN_3O_3Re$ C, 27.08; H, 2.50; N, 9.48. Found: C, 26.91; H, 2.44; N, 9.35.

3.4. *fac*-[ReCl(CO)$_3$(NH=C(Me)indz-κ^2*N,N*)], 3.

fac-[ReCl(CO)$_3$(NCMe)$_2$] (0.116 g, 0.3 mmol) and indazole (0.035 g, 0.3 mmol) were stirred in CH_3CN (15 mL) for 30 min at 60°C, then 0.016 mL of aqueous 0.02 M NaOH (0.003 mmol) was added and the solution was stirred for 30 min at 60°C. The volatiles were removed *in vacuo* and the yellow residue was crystallized from acetone/hexane at −20 °C, giving a yellow microcrystalline solid, which was decanted, washed with hexane (3 × 3 mL approximately), and dried *in vacuo*, yielding 0.126 g (91 %). IR (THF, cm^{-1}): 2020 vs, 1920 vs, 1891 vs. IR (KBr, cm^{-1}): 3178 m, 3116 w, 2021 vs, 1923 vs, 1885 br vs, 1637 m, 1583 w, 1560 w, 1542 w, 1511 m, 1481 m, 1464 m, 1424 m, 1354 m, 1283 w, 1214 w, 1196 m, 1089 w, 1044 w, 912 w, 874 w, 793 w, 757 m, 649 w, 324 w, 536 w, 519 w, 493 w, 470 w, 420 w. ^{1}H NMR (500 MHz, Me$_2$CO-d_6): 3.27 (s, NH=CCH_3, 3 H), 7.59 (t, *J* = 8 Hz, H^6 indz, 1 H), 7.83 (t, *J* = 8 Hz, H^5 indz, 1 H), 8.12 (d, *J* = 8 Hz, H^7 indz, 1 H), 8.18 (d, *J* = 8 Hz, H^4 indz, 1 H), 9.06 (s, H^3 indz, 1 H), 10.84 (br s, N*H*, 1 H). ^{13}C{^{1}H} NMR (126 MHz, Me$_2$CO-d_6): 20.1 (s, N=C*C*H$_3$), 112.3 (s, C^4H indz), 123.0 (C^7H indz), 125.3 (C^6H indz), 126.4 (C^{3a}H indz) 131.2 (C^5H indz), 139.0 (C^{7a}H indz), 143.9 (C^3H indz), 163.7 (N=*C*CH$_3$), *C*O were not observed due to the low solubility of the compound. Anal. Calcd. For $C_{12}H_9ClN_3O_3Re$ C, 30.97; H, 1.95; N, 9.03. Found: C, 31.31; H, 2.03; N, 8.88.

3.5. *fac*-[ReBr(CO)$_3$(NH=C(Ph)dmpz-κ^2*N,N*)], 7.

fac-[ReBr(CO)$_3$(NCMe)$_2$] (0.130 g, 0.3 mmol) and 3,5-dimethylpyrazole (0.029 g, 0.3 mmol) were stirred in

benzonitrile (5 mL) for 5 min at 80°C, then 0.053 ml of 0.056 M aqueous NaOH (0.003 mmol) was added, and the solution was stirred for 20 min at 80°C. The solvent was removed *in vacuo* and the yellow residue was crystallized from acetone/hexane at −20 °C, giving a yellow microcrystalline solid, which was decanted, washed with hexane (3 × 3 mL approximately), and dried *in vacuo*, yielding 0.076 g (46%). IR (THF, cm^{-1}): 2020 vs, 1920 vs, 1892 vs. IR (KBr, cm^{-1}): 3119 m, 3059 m, 2974 m, 2870 w, 2020 vs, 1914 vs, 1899 vs, 1638 m 1598 w, 1569 m, 1474 w, 1445 m, 1437 m, 1354 m, 1284 w, 1261 w, 1176 w, 1120 w, 1050 m, 1000 w, 949 w, 919 w, 886 w, 827 m, 803 w, 758 w, 709 m, 648 m, 635 w, 526 w, 496 w, 478 w. ^{1}H NMR (500 MHz, Me_2CO-d_6, 298 K): 1.85 (s, CH_3 dmpz, 3 H), 2.58 (s, CH_3 dmpz, 3 H), 6.47 (s, C^4H dmpz, 1 H), 7.54 (s br, *ortho*-C_6H_5, 1 H), 7.66-7.69 (m, *meta*-C_6H_5, 2 H), 7.74 (t, *J* = 7.5 Hz, *para*-C_6H_5, 1 H), 7.86 (s br, *ortho*-C_6H_5, 1H), 11.25 (s br, N*H*, 1 H). ^{1}H NMR (500 MHz, Me_2CO-d_6, 253 K): 1.84 (s, CH_3 dmpz, 3 H), 2.57 (s, CH_3 dmpz, 3 H), 6.51 (s, C^4H dmpz, 1 H), 7.52 (d, *J* = 9.0 Hz, *ortho*-C_6H_5, 1 H), 7.65-7.72 (m, *meta*-C_6H_5, 2 H), 7.75 (t, *J* = 7.5 Hz, *para*-C_6H_5, 1 H), 7.91 (d, *J* = 7.0 Hz, *ortho*-C_6H_5, 1 H), 11.40 (s, N*H*, 1 H). ^{13}C{^{1}H} NMR (126 MHz, Me_2CO-d_6): 14.2 (s, *C*H_3 dmpz), 16.2 (s, *C*H_3 dmpz), 114.2 (s, *C*^{4} dmpz), 129.2 (s, *ortho*-*C*$_6$H$_5$), 130.1 (s, *meta*-*C*$_6$H$_5$), 130.9 (s, *ipso*-*C*$_6$H$_5$), 133.0 (s, *para*-*C*$_6$H$_5$), 147.4 (s, *C*CH$_3$ dmpz), 157.7 (s, *C*CH$_3$ dmpz), 165.9 (s, NH=*C*(C$_6$H$_5$)), 188.9 (s, *C*O), 197.6 (s, *C*O), 198.4 (s, *C*O). Anal. Calcd. For $C_{15}H_{13}BrN_3O_3Re$ C, 32.79; H, 2.38; N, 7.65. Found: C, 33.07; H, 2,46; N, 7.77. This complex is rather unstable both in solid and in solution, so the NMR spectra of old samples maintained either in the solid state or in solution gave new unidentified signals. This instability precluded reliable measurement of its photophysical and electrochemical properties.

3.6. *fac*-[ReBr(CO)$_3$(NH=C(Ph)indz-κ^2*N*,*N*)], 8.

The same procedure as for **7**, using indazole (0.035 g, 0.3 mmol) as starting material, gave 0.087 g (51 %) of **8** as a yellow microcrystalline solid. IR (THF, cm^{-1}): 2022 vs, 1925 vs, 1896 vs. IR (KBr, cm^{-1}): 3448 m, 3370 m, 2023 vs, 1930 vs, 1881 vs, 1617 m, 1498 w, 1455 m, 1441 m, 1351 w, 1331 w, 1267 w, 1107 w, 1053 w, 919 w, 900 w, 789 w, 757 m, 706 w, 644 w, 623 w, 527 w, 493 w, 422 w. ^{1}H NMR (500 MHz, Me_2CO-d_6, 298 K): 6.45 (d, *J* = 8.5 Hz, C^4H indz, 1 H), 7.49-7.50 (m, C^5H and C^6H indz, 2 H), 7.66 (s br, *ortho*-C_6H_5, 1 H), 7.78 (m, *meta*-C_6H_5, 2 H), 7.87 (t, *J* = 7.5 Hz, *para*-C_6H_5, 1 H), 7.98 (s br, *ortho*-C_6H_5, 1 H), 8.09 (d, *J* = 8.5 Hz, C^7H indz, 1H), 9.20 (s, C^3H indz, 1 H), 11.28 (s, N*H*, 1 H). ^{1}H NMR (500 MHz, Me_2CO-d_6, 253 K): 6.43 (d, *J* = 8.0 Hz, C^4H indz, 1 H), 7.51-7.53 (m, C^5H and C^6H indz, 2 H), 7.64 (d, *J* = 7.5 Hz, *ortho*-C_6H_5, 1 H), 7.79 (m, *meta*-C_6H_5, 2 H), 7.88 (t, *J* = 7.5 Hz, *para*-C_6H_5, 1 H), 8.03 (d, *J* = 8.0 Hz, *ortho*-C_6H_5, 1 H), 8.10 (d, *J* = 8.0 Hz, C^7H indz, 1H), 9.28 (s, C^3H indz, 1 H), 11.43 (s, N*H*, 1 H). ^{13}C{^{1}H} NMR (126 MHz, Me_2CO-d_6): 113.6 (s, *C*^{4}H indz), 124.4 (s, *C*^{7}H indz), 127.0 (s, *C*^{6}H indz), 128.3 (s, *C*^{3a} indz), 130.1 (s, *ortho*-*C*$_6$H$_5$), 131.0 (s, *ipso*-*C*$_6$H$_5$), 131.2 (s, *meta*-*C*$_6$H$_5$), 132.6 (s, *C*^{5}H indz), 134.3 (s, *para*-*C*$_6$H$_5$), 141.3 (s, *C*^{7a} indz), 146.7 (s, *C*^{3}H indz), 165.6 (s, NH=*C*(C$_6$H$_5$)), 189.9 (*C*O), 198.2 (*C*O), 198.3 (*C*O). Anal. Calcd. For $C_{17}H_{11}BrN_3O_3Re$ C, 35.73; H, 1.94; N, 7.36. Found: C, 35.92; H, 2.01; N, 7.29.

3.7. Photophysical Experiments.

UV-vis spectra were measured with a VARIAN-Cary 100 Spectrophotometer and emission spectra were recorded on a Jobin-Yvon FluoroLog 3.2.2 in CH_2Cl_2 at room temperature. Luminescence lifetimes were measured on a spectrofluorimeter Edinburgh Instrument Fl-900, using software with time-correlated single photon mode coupled to a Stroboscopic system. The excitation source was a laser diode (λ 320 nm). The instrument response function was determined by using a light-scattering solution (LUDOX).

3.8. Electrochemical Experiments.

Voltammetric analyses were carried out in a standard three-electrode cell with a Radiometer PGP 201 potentiostat at ambient temperature. The electrolyte consisted of 0.2 M $N^nBu_4PF_6$ solution in MeCN or CH_2Cl_2. The working electrode was a platinum disk electrode and the auxiliary electrode was a platinum wire. The reference electrode was a silver-silver ion electrode, Ag/Ag^+ (0.1 M $AgClO_4$ in MeCN) separated from the analyzed solution by a sintered glass disk. After each measurement the reference was checked against the ferrocene-ferricinium couple (+0.025 V and +0.16 V against this reference electrode in MeCN and in CH_2Cl_2 solution respectively).

3.9. Computational Details.

All calculations have been performed using the Gaussian 09 program package,[29] in which the PBE1PBE method was applied. This hybrid Hartree-Fock/ density functional model is based on the Perdew-Burke-Erzenhof (PBE) functional,[30] where the HF/DFT exchange ratio is fixed a priori to 1/4, and was used to optimize the ground and excited state geometries. Geometry optimizations were performed under no symmetry restrictions, using initial coordinates derived from X-ray data of the same complexes when availables, and frecuency analyses were performed to ensure that a minimum structure with no imaginary frecuencies was achieved in each case. On the basis of the optimized ground and excited state geometries, the absorption and emission properties in dichloromethane solution were calculated by TD-DFT[31] at the PBE1PBE level associated with the PCM method to introduce the solvent effects.[32] Spin-orbital coupling is not included in the current TD-DFT method, and it influences the excitation energies in which the Re electrons are involved,[33] whereas it has a negligible effect on the transition character of this complexes. Hence, although TD-DFT cannot exactly estimate the excitation energies, it can still provide a reasonable spectral feature for our investigated complexes. This kind of theoretical approach has been proven to be reliable for transition-metal complex systems.[34] In the calculations, effective core potentials (ECP) and their associated double-ζ LANL2DZ basis set were used for the rhenium and bromide atoms,[35] while the light elements (O, N, C, and H) were described with the 6-31+G(d,p) basis.[36] To

explain the rationality of the PBE1PBE method and LANL2DZ/6-31+G(d,p) basis set, complex **1** was selected to do the calculation test with different functionals and basis sets. Table S1 (ESI) show the main bond distances obtained by LANL2DZ/6-31+G(d,p) basis set with different functionals, being the results obtained with PBE1PBE between the most accurate. The calculated results obtained by other larger basis sets including SDD/6-311+G(d,p) and def2-TZVPP[37] are gathered in Table S2, and no significant improvement in the accuracy is detected, therefore, the LANL2DZ/6-31+G(d,p) basis set was selected to perform the calculations without the computational cost demanded by the larger basis sets. The contribution of every fragment in the molecules studied to the different orbitals involved in the optical transitions was calculated with the AOMix program,[38] and the graphical representation of the orbitals was made with the help of GaussView.[39]

3.10. Crystal Structure Determination for Compounds 1, 2, and 7.

Crystals were grown by slow diffusion of hexane into concentrated solutions of the complexes in acetone (for **1**) or THF (for **2**, and **7**) at −20 °C. Relevant crystallographic details can be found in the CIF.† A crystal was attached to a glass fiber and transferred to an Agilent SuperNova diffractometer fitted with an Atlas CCD detector. The crystals were kept at 293(2) K during data collection. Using Olex2,[40] the structure was solved for complexes **1** and **7** with the olex2.solve structure solution program,[41] or with the ShelXT structure solution program for complex **2**,[42] and then the structures were refined with the ShelXL refinement package using Least Squares minimisation.[43] All non-hydrogen atoms were refined anisotropically. Hydrogen atoms were set in calculated positions and refined as riding atoms, with a common thermal parameter. All graphics were made with Olex2, and distances and angles of hydrogen bonds were calculated with PARST[44] (normalized values).[45]

4. Conclusions

Novel neutral and cationic rhenium(I) pyrazolylamidino complexes have been synthesized and characterized. The main advantage of pyrazolylamidino with respect to other bidentate chelating *N*-donor ligands is the facile introduction of different substituents starting from the appropriate pyrazole and nitrile. Once coordinated, the pyrazolylamidino ligand is robust enough to allow the substitution of the halide by another halide or by different neutral ligands, so a broad panel of chelate complexes with different substituents are easily obtained. The effect of several substituents at the pyrazolylamidino ligand has been evaluated, as well as the effect of the coordination of chlorido *vs.* bromido, and their substitution by neutral acetonitrile or pyrazole ligands yielding cationic complexes. All the complexes exhibit phosphorescence decays, their quantum yields and long lifetimes are similar to those of other literature-known rhenium(I) tricarbonyl complexes, and proof that emission arises from a prevalently ^{3}MLCT state. The electrochemical study reveals an irreversible reduction for all the complexes. The oxidation of the neutral complexes was found to be irreversible due to halido dissociation, whereas the cationic species display a reversible process implying the Re^{I}/Re^{II} couple. Finally, TD-DFT methods provide reasonable values for emission energies, which follow the same trend of experimental values of the emission wavelengths. Therefore, this report opens a new strategy to design new versatile phosphorescent complexes of the rhenium(I)tricarbonyl family, since targeted chelating *N*-donor ligand with the appropriate substituents for requested applications may be easily obtained in a one-pot reaction from readily available pyrazole and nitrile ligands.

Acknowledgements

This research was supported by the Spanish MINECO (Project CTQ2013-41067-P). P. G.-I. thanks the UVa for her grant. The authors in France thank the CNRS for financial support.

Notes and references

‡ As shown in Table 3, compound **7** displays a second wave at −2.14 V, whereas a second wave at potential lower than the lower limit recorded (below −2.5 V) may be also perceived for compound **8**. Therefore, this second wave might be attributed to the presence of a phenyl substituent in the pyrazolylamidino ligand.

§ Complex **3** should present the same behaviour as **6** or **10** but the $E^{1/2}_{ox}$ was not clear in the CV probably due to the low solubility of this compound in MeCN (as indicated in footnote in Table 3).

1 (a) M. Wrighton and D. L. Morse, *J. Am. Chem. Soc*., 1974, **96**, 998–1003. (b) P. Giordano, S. Fredericks, M. S. Wrighton and D. Morse, *J. Am. Chem. Soc*., 1978, **100**, 2257–2259. (c) J. C. Luong, L. Nadjo and M. S. Wrighton, *J. Am. Chem. Soc*., 1978, **100**, 5790–5795.

2 Some reference reviews: (a) A. J. Lees, *Chem. Rev*., 1987, **87**, 711−743. (b) D. J. Stufkens, *Comments Inorg. Chem*., 1992, **13**, 359–385. (c) A. I. Baba, J. R. Shaw, J. A. Simon, R. P. Thummel and R. H. Schmehl, *Coord. Chem. Rev.,* 1998, **171**, 43-59. (d) V. W.-W. Yam, *Chem. Commun.*, 2001, 789-796; (e) A. Coleman,C. Brennan,J. G. Vos and M. T. Pryce, *Coord. Chem. Rev*., 2008, **252**, 2585−2595. (f) A. Kumar, S.-S. Sun and A. J. Lees, *Top. Organomet. Chem*., 2010, **29**, 1−35. (g) A. Vlček Jr., *Top. Organomet. Chem*., 2010, **29**, 73−114.

3 Some reference articles: (a) L. A. Worl, R. Duesing, P. Chen, L. D. Ciana and T. J. Meyer, *J. Chem. Soc., Dalton Trans*., 1991, 849-858. (b) L. Sacksteder, M. Lee, J. N. Demas and B. A. DeGraff, *J. Am. Chem. Soc*., 1993, **115**, 8230-8238. (c) H. Hori, F. P. A. Johnson, K. Koike, K. Takeuchi, T. Ibusuki and O. Ishitani, *J. Chem. Soc.,Dalton Trans*., 1997, 1019-1023. (d) L. Sacksteder, A. P. Zipp, E. A. Brown, J. Streich, J. N. Denas and B. A. DeGraff, *Inorg. Chem*., 1990, **29**, 4335-4340. (e) V. W.-W. Yam, V. C.-Y. Lau and K.-K. Cheung, *Organometallics*, 1995, **14**, 2749-2753. (f) T. A. Oriskovich, P. S. White and H. H. Thorp, *Inorg. Chem*., 1995, **34**, 1629-1631. (g) W. B. Connick, A. J. Di Bilio, M. G. Hill, J. R. Winkler and H. B. Gray, *Inorg. Chim. Acta*, 1995, **240**, 169-173. (h) R. V. Slone, D. I. Yoon, R. M. Calhoun and J. T. Hupp, *J. Am. Chem. Soc*., 1995, **117**, 11813-11814. (i) R. L. Cleary, K. J. Byrom, D. A. Bardwell,

J. C. Jeffery, M. D. Ward, G. Calogero, N. Armaroli, L. Flamigni and F. Barigelletti, *Inorg. Chem*., 1997, **36**, 2601-2609. (j) S.-S. Sun and A. J. Lees, *J. Am. Chem. Soc.*, 2000, **122**, 8956-8967. (k) J. M. Villegas, S. R. Stoyanov, W. Huang and D. P. Rillema, *Dalton Trans.*, 2005, 1042-1051. (l) J. M. Villegas, S. R. Stoyanov, W. Huang and D. P. Rillema, *Inorg. Chem*., 2005, **44**, 2297-2309. (m) C.-C. Ko, W.-M. Kwok, V. W.-W. Yam and D. L. Phillips, *Chem. Eur. J.*, 2006, **12**, 5840–5848. (n) D. V. Partyka, N. Deligonul, M. P. Washington and T. G. Gray, *Organometallics*, 2009, **28**, 5837–5840. (o) M.-J. Li, X. Liu, Y.-Q. Shi, R.-J. Xie, Q.-H. Weia and G.-N. Chen, *Dalton Trans.*, 2012, **41**, 10612–10618. (p) D. Chartrand, C. A. Castro Ruiz and G. S. Hanan, *Inorg. Chem*., 2012, **51**, 12738−12747. (q) C. B. Anderson, A. B. S. Elliott, C. J. McAdam, K. C. Gordon and J. D. Crowley, *Organometallics*, 2013, **32**, 788−797. (r) N. Saleh, M. Srebro, T. Reynaldo, N. Vanthuyne, L. Toupet, V. Y. Chang, G. Muller, J. A. G. Williams, C. Roussel, J. Autschbach, J. Crassous, *Chem. Commun.,* 2015, **51**, 3754-3757.

4 Some reference reviews: (a) K. S. Schanze, D. B. MacQueen, T. A. Perkins and T. A. Cabana, *Coord. Chem. Rev*., 1993, **122**, 63–89. (b) P. Chen and T. J. Meyer, *Chem. Rev*., 1998, **98**, 1439−1477. (c) D. J. Stufkens, A. Vlček Jr., *Coord. Chem. Rev*., 1998, **177**, 127−179. (d) D. R. Striplin and G. A. Crosby, *Coord. Chem. Rev.*, 2001, **211**, 163– 175.

5 R. A. Kirgan, B. P. Sullivan and D. P. Rillema, *Top. Curr. Chem*., 2007, **281**, 45–100.

6 Some reference reviews: (a) K. K.-W. Lo, W.-K. Hui, C.-K. Chung, K. H.-K. Tsang, T. K.-M. Lee, C.-K. Li, J. S.-Y. Lau, and D. C.-M. Ng, *Coord. Chem. Rev*., 2006, **250**, 1724–1736. (b) C. Beck, J. Brewer, J. Lee, D. McGraw, B. A. DeGraff and J. N. Demas, *Coord. Chem. Rev*., 2007, **251**, 546–553. (c) V. Fernández-Moreira, F. L. Thorp-Greenwood and M. P. Coogan, *Chem. Commun*., 2010, **46**, 186–202. (d) K. K.-W. Lo, M.-W. Louie and K. Y. Zhang, *Coord. Chem. Rev.*, 2010, **254**, 2603−2622. (e) K. K.-W. Lo, *Top. Organomet. Chem*., 2010, **29**, 115−158. (f) R. Balasingham, M. P. Coogan and F. L. Thorp-Greenwood, *Dalton Trans*., 2011, **40**, 11663−11674. K.-W.Lo, K. Y. Zhang, S. P.-Y. Li, *Eur. J. Inorg. Chem*., 2011, 3551−3568. (h) K. K.-W. Lo, A. W.-T. Choi and W. H.-T. Law, *Dalton Trans.*, 2012, **41**, 6021−6047.

7 Review: H. Takeda and O. Ishitani, *Coord. Chem. Rev.*, 2010, **254**, 346−354.

8 Review: H. Yersin, A. F. Rausch, R. Czerwieniec, T. Hofbeck and T. Fischer, *Coord. Chem. Rev.*, 2011, **255**, 2622–2652.

9 Some reference reviews: (a) K. S. Schanze, D. B. MacQueen, T. A. Perkins and L. A. Cabana, *Coord. Chem. Rev.*, 1993, **122**, 63–89. (b) A. S. Polo, M. K. Itokazu, K. M. Frin, A. O. de T. Patrocínio and N. Y. M. Iha, *Coord. Chem. Rev.*, 2006, **250**, 1669−1680.

10 (a) C.-C. Hsieh, C.-J. Lee and Y.-C. Horng, *Organometallics*, 2009, **28**, 4923-4928. (b) A. V. Khripun, V. Y. Kukushkin, S. I. Selivanov, M. Haukka and A. J. L. Pombeiro, *Inorg. Chem.*, 2006, **45**, 5073-5083. (c) E. Reisner, V. B. Arion, A. Rufinsha, I. Chiorescu, W. E. Schmid and D. K. Keppler, *Dalton Trans.*, 2005, 2355-2364. (d) P. Govidaswamy, Y. A. Mozharivskyj and M. R. Kollipara, *J. Organomet. Chem.*, 2004, **689**, 3265-3274. (e) M. R. Kollipara, P. Sarkhel, S. Chakraborty and R. Lalrempuia, *J. Coord. Chem*., 2003, **56**, 1085-1091. (f) D. Carmona, J. Ferrer, F. J. Lahoz, L. A. Oro and M. P. Lamata, *Organometallics*, 1996, **15**, 5175-5178. (g) J. López, A. Santos, A. Romero and A. M. Echavarren, *J. Organomet. Chem.,* 1993, **443**, 221-228. (h) M. A. Cinellu, S. Stoccoro, G. Minghetti, A. L. Bandini, G. Banditelli and B. Bovio, *J. Organomet. Chem.*, 1989, **372**, 311-325. (i) M. O. Albers, S. Francesca, A. Crosby, D. C. Liles, D. J. Robinson, A. Shaver and E. Singleton, *Organometallics*, 1987, **6**, 2014-2017.(j) G. D. Gracey, S. T. Rettig, A. Storr and J. Trotter, *Can. J. Chem.*, 1987, **65**, 2469-2477. (k) A. Romero, A. Vegas, A. Santos, *J. Organomet. Chem.*, 1986, **310**, C8-C10. (l) C. J. Jones, J. A. McCleverty and A. S. Rothin, *J. Chem. Soc., Dalton Trans.*, 1986, 109-111.

11 (a) M. Arroyo, P. Gómez-Iglesias, J. M. Martín-Alvarez, C. M. Alvarez, D. Miguel and F. Villafañe, *Inorg. Chem*., 2012, **51**, 6070-6080. (b) N. Antón, M. Arroyo, P. Gómez-Iglesias, D. Miguel and F. Villafañe, *J. Organomet. Chem*., 2008, **693**, 3074-3080. (c) M. Arroyo, D. Miguel, F. Villafañe, S. Nieto, J. Pérez and L. Riera, *Inorg. Chem.*, 2006, **45**, 7018-7026. (d) M. Arroyo, A. López-Sanvicente, D. Miguel and F. Villafañe, *Eur. J. Inorg. Chem.*, 2005, 4430-4437.

12 P. Gómez-Iglesias, M. Arroyo, S. Bajo, C. Strohmann, D. Miguel and F. Villafañe, *Inorg. Chem*., 2014, **53**, 12437−12448.

13 (a) G. A. Jeffrey, *An Introduction to Hydrogen Bonding*; Oxford University Press: New York, 1997; Chapter 2. (b) T. Steiner, *Angew. Chem., Int. Ed*., 2002, **41**, 48−76.

14 (a) K. Kalyanasundaram, *J. Chem. Soc., Faraday Trans. 2*, 1986, **82**, 2401-2415. (b) W.-K. Chu, C.-C. Ko, K.-C. Chan, S.-M. Yiu, F.-L. Wong, C.-S. Lee and V. A. L. Roy, *Chem. Mater.*, 2014, **26**, 2544-2550.

15 J. G. Vaughan, B. L. Reid, P. J. Wright, S. Ramchandani, B. M. Skelton, P. Raiteri, S. Muzzioli, D. H. Brown, S. Stagni and M. Massi, *Inorg. Chem*., 2014, **53**, 3629−3641.

16 H. C. Bertrand, S. Clède, R. Guillot, F. Lambert and C. Policar, *Inorg. Chem*., 2014, **53**, 6204-6223.

17 D. Donghi, G. D'Alfonso, M: Mauro, M. Panigati, P. Mercandelli, A. Sironi, P. Mussini and L. D'Alfonso, *Inorg. Chem.,* 2008, **47**, 4243-4255.

18 D. Magde, J. H. Brannon, T. L. Cremers and J. Olmsted, *J. Phys. Chem.*, 1979, **83**, 696-699.

19 (a) V. W.-W. Yam, B. Li, Y. Yang, B. W.-K. Chu, K. M.-C. Wong and K.-K. Cheung, *Eur. J. Inorg. Chem.*, 2003, 4035-4042. (b) S. Ranjan, S.-Y. Lin, K.-C. Hwang, Y. Chi, W.-L. Ching, C.-S. Liu, Y.-T. Tao, C.-H. Chien, S.-M. Peng and G.-H. Lee, *Inorg. Chem*., 2003, **42**, 1248-1255. (c) O. S. Wenger, L. M. Henling, M. W. Day, J. R. Winkler and H. B. Gray, *Inorg Chem*., 2004, **43**, 2043-2048. (d) H. Tsubaki, A. Sekine, Y. Ohashi, K. Koike, H. Takeda and O. Ishitani, *J. Am. Chem. Soc.*, 2005, **127**, 15544-15555. (e) N. J. Lundin, A. G. Blackman, K. C. Gordon and D. L. Officer, *Angew. Chem. Int. Ed.*, 2006, **45**, 2582-2584.

20 J. R. Lacowicz, *Principles of Fluorescence Spectroscopy*, 2nd ed.; Kluwer: New York, 1999.

21 (a) P. J. Giordano and M. S. Wrighton, *J. Am. Chem. Soc.*, 1979, **101**, 2888-2897. (b) A. Juris, V. S. Campagna, I. Bidd, J.-M. Lehn and R. Ziessel, *Inorg. Chem.*, 1988, **27**, 4007-4011. (c) T. G. Kotch, A. J. Lees, S. J. Fuerniss and K. I. Papathomas, *Chem. Mater.*, 1992, **4**, 675-683. (d) A. Vogler and H. Kunkely, *Coord. Chem. Rev.*, 2000, **200-202**, 991-1008. (e) T. Doleck, J. Attard, F. R. Fronczek, A. Moskun and R. Isovitsch, *Inorg. Chim. Acta*, 2009, **362**, 3872-3876.

22 See for example: (a) G. J. Stor, F. Hartl, J. W. M. van Outersterp and D. J. Stufkens, *Organometallics*, 1995, **14**, 1115-1131. (b) B. D. Rossenaar, F. Hartl and D. J. Stufkens, *Inorg. Chem.*, 1996, **35**, 6194-6203. (c) A. Klein, C. Vogler and W. Kaim, *Organometallics*, 1996, **15**, 236-244.

23 P. Christensen, A. Hamnett, A. V. G. Muir and J. A. Timney, *J. Chem. Soc., Dalton Trans*., 1992, 1455-1463.

24 F. Magno, C.-A. Mazzocchin and G. Bontempelli, *J. Electroanal. Chem.*, 1973, **47**, 461-468.

25 A. Drozdz, M. Bubrin, J. Fiedler, S. Záliš and W. Kaim, *Dalton Trans.*, 2012, **41**, 1013-1019.

26 G. A. Ardizzoia, G. LaMonica, A. Maspero, M. Moret and N. Masciocchi, *Eur. J. Inorg. Chem.*, 1998, 1503−1512.

27 D. D. Perrin and W. L. F. Armarego, "*Purification of Laboratory Chemicals*"; 3rd ed.; Pergamon Press: Oxford, 1988.

28 M. F. Farona and K. F. Kraus. *Inorg. Chem.*, 1970, **9**, 1700-1704.
29 Gaussian 09, Revision A.02, M. J. Frisch, G. W. Trucks, H. B. Schlegel, G. E. Scuseria, M. A. Robb, J. R. Cheeseman, G. Scalmani, V. Barone, B. Mennucci, G. A. Petersson, H. Nakatsuji, M. Caricato, X. Li, H. P. Hratchian, A. F. Izmaylov, J. Bloino, G. Zheng, J. L. Sonnenberg, M. Hada, M. Ehara, K. Toyota, R. Fukuda, J. Hasegawa, M. Ishida, T. Nakajima, Y. Honda, O. Kitao, H. Nakai, T. Vreven, J. A. Montgomery Jr., J. E. Peralta, F. Ogliaro, M. Bearpark, J. J. Heyd, E. Brothers, K. N. Kudin, V. N. Staroverov, R. Kobayashi, J. Normand, K. Raghavachari, A. Rendell, J. C. Burant, S. S. Iyengar, J. Tomasi, M. Cossi, N. Rega, J. M. Millam, M. Klene, J. E. Knox, J. B. Cross, V. Bakken, C. Adamo, J. Jaramillo, R. Gomperts, R. E. Stratmann, O. Yazyev, A. J. Austin, R. Cammi, C. Pomelli, J. W. Ochterski, R. L. Martin, K. Morokuma, V. G. Zakrzewski, G. A. Voth,P. Salvador, J. J. Dannenberg, S. Dapprich, A. D. Daniels, O. Farkas, J. B. Foresman, J. V. Ortiz, J. Cioslowski and D. J. Fox, Gaussian, Inc., Wallingford CT, 2009.
30 (a) J. P. Perdew, K. Burke and M. Ernzerhof, *Phys. Rev. Lett.*, 1996, **77**, 3865-3868. (b) J. P. Perdew, K. Burke, and M. Ernzerhof, *Phys. Rev. Lett.*, 1997, **78**, 1396. (c) C. Adamo and V. Barone, *J. Chem. Phys.*, 1999, **110**, 6158-6170.
31 (a) T. Helgaker and P. Jorgensen, *J. Chem. Phys.*, 1991, **95**, 2595-2601. (b) K. L. Bak, P. Jorgensen, T. Helgaker, K. Rund, and H. J. A. Jenson, *J. Chem. Phys.*, 1993, **98**, 8873-8887. (c) J. Autschbach, T. Ziegler, S. J. A. Gisbergen and E. J. Baerends, *J. Chem. Phys.*, 2002, **116**, 6930-6940.
32 (a) E. Cances, B. Mennucci and J. Tomasi, *J. Chem. Phys.*, 1997, **107**, 3032-3041. (b) M. Cossi, V. Barone, B. Mennucci and J. Tomasi, *Chem. Phys. Lett*. 1998, **286**, 253-260. (c) B. Mennucci and J. Tomasi, *J. Chem. Phys.*, 1997, **106**, 5151-5158.
33 L.-L. Shi, Y. Liao, L. Zhao, Z.-M. Su,Y.-H. Kan, G.-C. Yang and S.Y. Yang, *J. Organomet. Chem.*, 2007, **692**, 5368-5374.
34 (a) S. R. Stoyanov, J. M. Villegas and D. P. Rillema, *Inorg. Chem.*, 2002, **41**, 2941-2945. (b) D. Di Censo, S. Fantacci, F. De Angelis, C. Klein, N. Evans, K. Kalyanasundaram, H. J. Bollink, M. Gratzel and M. K. Nazeeruddin, *Inorg. Chem.*, 2008, **47**, 980-989. (c) T. H. Kwon, H. S. Cho, M. K. Kim, J. W. Kim, J. J. Kim, K. H. Lee, S. J. Park, I. S. Shin, H. Kim, D. M. Shin, Y. K. Chung and J. I. Hong, *Organometallics*, 2005, **24**, 1578-1585. (d) Q. Zhao, S. Liu, M. Shi, C. Wang, M. Yu, L. Li, F. Li, T. Yi and C. Huang, *Inorg. Chem.*, 2006, **45**, 6152-6160. (e) K. Zheng, J. Huang, W. Peng, X. Liu and F. Yun, *J. Phys. Chem. A*, 2001, **105**, 10899-10905. (f) K. Zheng, J. Huang, Y. Shen, D. Kuang and F. Yun, *J. Phys. Chem. A*, 2001, **105**, 7248-7253. (g) A. Vlček Jr. and S. Zalis, *J. Phys. Chem. A*, 2005, **109**, 2991-2992.
35 (a) P. J. Hay and W. R. Wadt, *J. Chem. Phys.*, 1985, **82**, 270-283. (b) P. J. Hay and W. R. Wadt, *J. Chem. Phys.*, 1985, **82**, 299-310.
36 (a) A. Gabrielsson, P. Matousek, M. Towrie, F. Hartl, S. Zalis, A. Vlček Jr., *J. Phys. Chem. A*, 2005, **109**, 6147-6153. (b) D. M. Dattelbaum, K. M. Omberg, P. J. Hay, N. L. Gebhart, R. L. Martin, J. R. Schoonover and T. J. Meyer, *J. Phys. Chem. A*, 2004, **108**, 3527-3536. (c) D. M. Dattelbaum, R. L. Martin, J. R. Schoonover and T. J. Meyer, *J. Phys. Chem. A*, 2004, **108**, 3518-3526. (d) N. J. Lundin, P. J. Walsh, S. L. Howell, J. J. McGarvey, A. G. Blackman and K. C. Gordon, *Inorg. Chem.*, 2005, **44**, 3551-3560.
37 (a) T. H. Dunning Jr. and P. J. Hay, in *Modern Theoretical Chemistry*, Ed. H. F. Schaefer III, Vol. 3 (Plenum, New York, 1977), 1-28. (b) U. Wedig, M. Dolg, H. Stoll and H. Preuss, in *Quantum Chemistry: The Challenge of Transition Metals and Coordination Chemistry*, Ed. A. Veillard, Reidel, and Dordrecht (1986) 79. (c) F. Weigend and R. Ahlrichs, *Phys. Chem. Chem. Phys.*, 2005, **7**, 3297-3305. (d) D. Andrae, U. Haeussermann, M. Dolg, H. Stoll and H. Preuss, *Theor. Chim. Acta*, 1990, **77**, 123-141.
38 (a) S. I. Gorelsky, *AOMix: Program for Molecular Orbital Analysis*, http://www.sg-chem.net/, University of Ottawa, version 6.5, 2011. (b) S. I. Gorelsky and A. B. P. Lever, *J. Organomet. Chem.*, 2001, **635**, 187-196.
39 GaussView, Version 5, R. Dennington, T. Keith and J. Millam, *Semichem Inc.*, Shawnee Mission KS, 2009.
40 O. V. Dolomanov, L. J. Bourhis, R. J. Gildea, J. A. K. Howard and H. Puschmann, *J. Appl. Cryst.*, 2009, **42**, 339-341.
41 L. J. Bourhis, O. V. Dolomanov, R. J. Gildea, J. A. K. Howard and H. Puschmann, *Acta Cryst.*, 2015, **A71**, 59-75.
42 G. M. Sheldrick, *Acta Cryst.*, 2015, **A71**, 3-8.
43 G. M. Sheldrick, *Acta Cryst.*, 2008, **A64**, 112-122.
44 (a) M. Nardelli, *Comput. Chem.*, 1983, **7**, 95−98. (b) M. Nardelli, *J. Appl. Crystallogr.*, 1995, **28**, 659.
45 (a) G. A. Jeffrey and L. Lewis, *Carbohydr. Res.*, 1978, **60**, 179−182. (b) R. Taylor and O. Kennard, *Acta Crystallogr.*, 1983, **B39**, 133−138.

Electronic Supplementary Information

Luminescent Rhenium(I) Tricarbonyl Complexes with Pyrazolylamidino Ligands: Photophysical, Electrochemical, and Computational Studies

Patricia Gómez-Iglesias, Fabrice Guyon, Abderrahim Khatyr, Gilles Ulrich, Michael Knorr, Jose Miguel Martín-Alvarez, Daniel Miguel, and Fernando Villafañe*

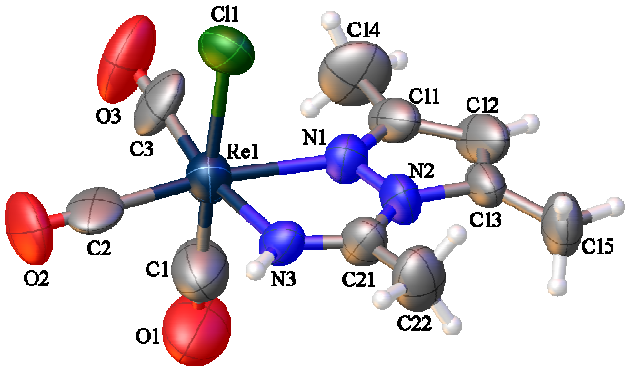

Figure S1. Perspective view of *fac*-[ReCl(CO)$_3$(NH=C(Me)dmpz-κ^2*N,N*)], **2,** showing the atom numbering. Thermal ellipsoids are drawn at 50% probability.

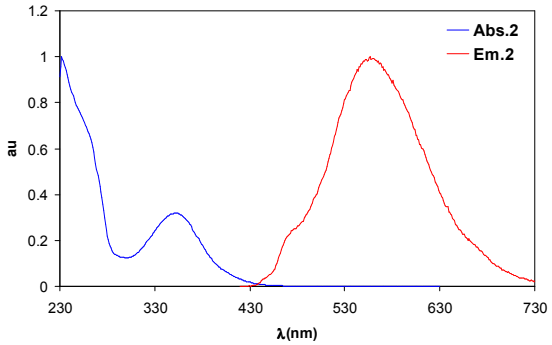
Abs.2
Em.2
au
λ(nm)

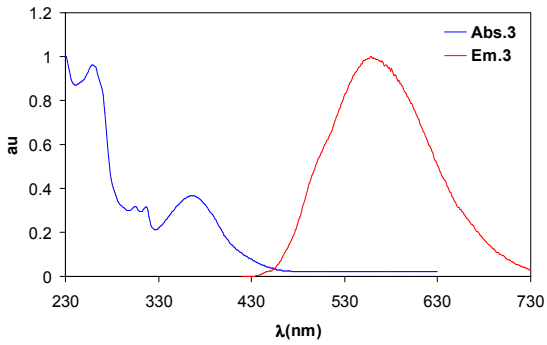
Abs.3
Em.3
au
λ(nm)

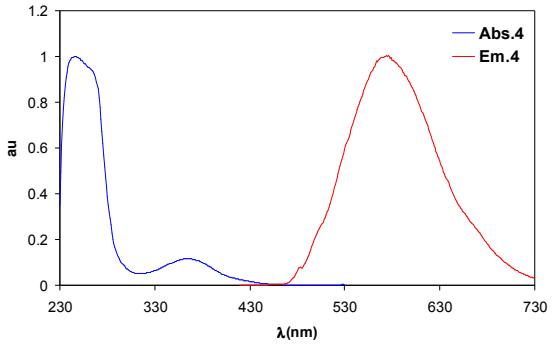
Abs.4
Em.4
au
λ(nm)

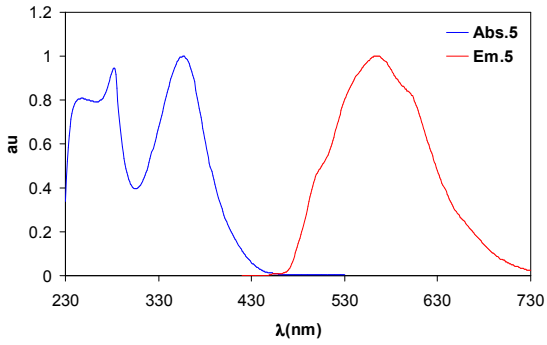
Abs.5
Em.5
au
λ(nm)

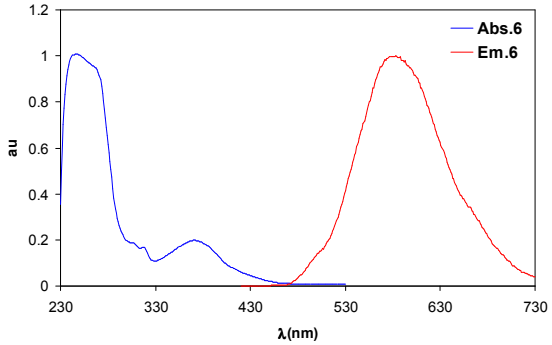
Abs.6
Em.6
au
λ(nm)

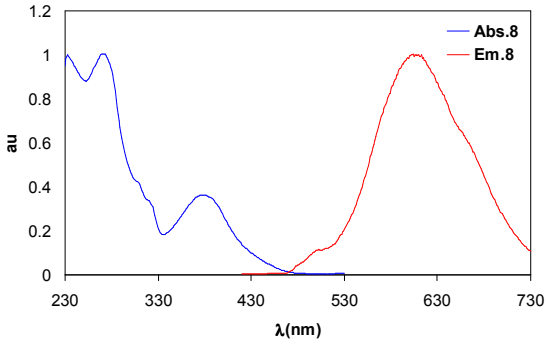
Abs.8
Em.8
au
λ(nm)

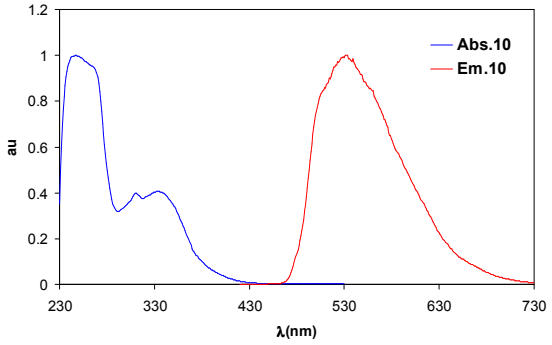
Abs.10
Em.10
au
λ(nm)

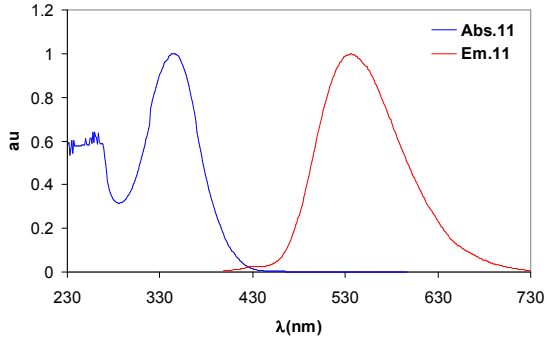
Abs.11
Em.11
au
λ(nm)

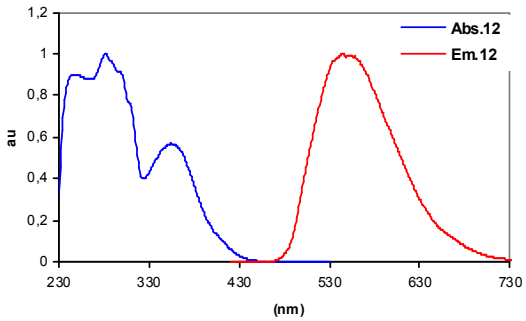

Figure S2. Normalized emission (red) and absorption (blue) spectra recorded in CH_2Cl_2 of complexes **2**-**6**, **8**, **10**-**12** at 298 K. As indicated in Table 1, not reliable spectra could be obtained for **7** due to its instability in CH_2Cl_2 solution.

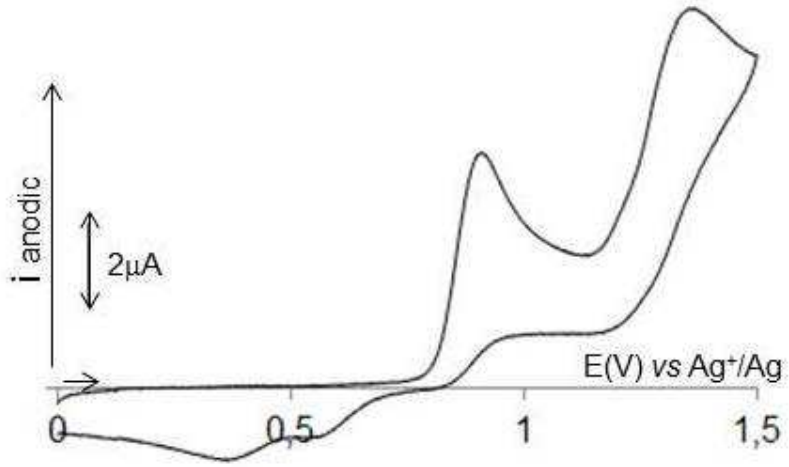

Figure S3. Cyclic voltammogram recorded in CH_2Cl_2 solution of 10 mM **5**. Scan rate: 100 mV/s.

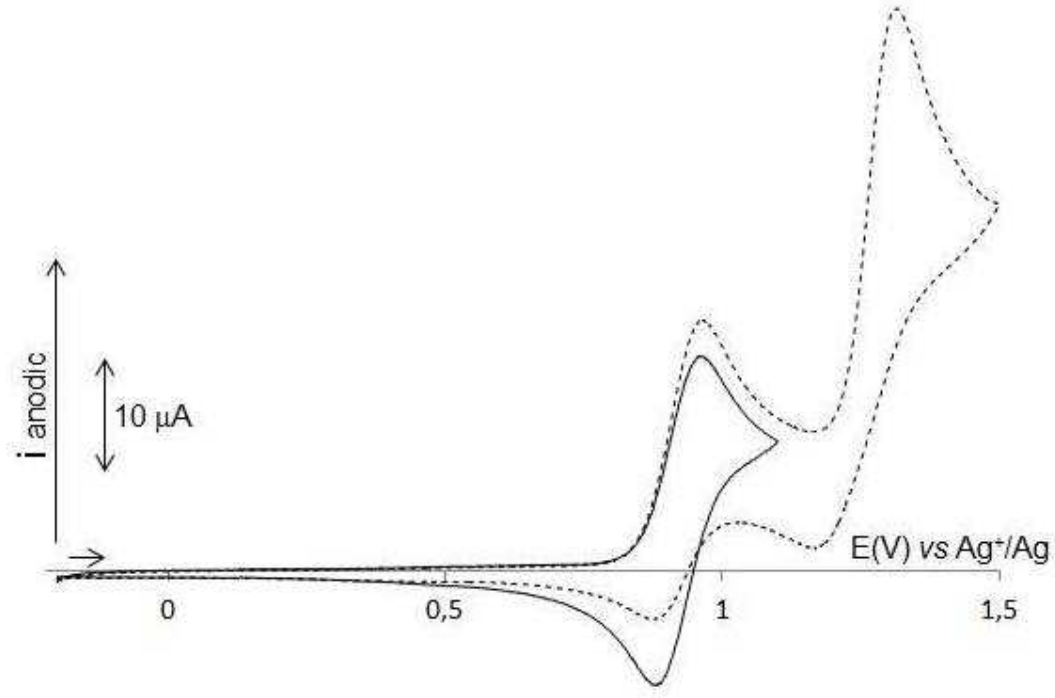

Figure S4. Cyclic voltammogram recorded in MeCN solution of 8.6 mM *fac*-$[ReBr(CO)_3(dmpzH)_2]$. Scan rate: 100 mV/s.

Table S1. Deviation from the geometry found by X-ray diffraction for selected bond distances of complex **1** calculated with different functionals and using LANL2DZ for the Re atom and 6-31G+(d,p) for the rest of the atoms (Calculated distance - experimental distance).

Functional	Re1-Cl1	Re1-N3	Re1-N1	Re1-C1	Re1-C2	Re1-C3	Average deviation
B3LYP	0.040	0.008	0.010	0.005	0.041	0.002	0.018
BMK	0.036	0.010	0.011	0.011	0.047	0.006	0.020
CAM-B3LYP	0.022	0.003	-0.002	-0.003	0.038	-0.004	0.012
M06	0.019	0.009	-0.002	-0.0002	0.038	-0.005	0.012
PBE	0.019	-0.013	-0.008	0.003	0.034	-0.005	0.014
TPSS	0.018	-0.016	-0.014	0.010	0.043	0.004	0.018
WB97XD	0.026	0.012	0.002	-0.010	0.032	-0.011	0.016
PBE1PBE	-0,003	-0.018	-0.021	-0.008	0.030	-0.011	0.015

Table S2. Deviation from the geometry found by X-ray diffraction for selected bond distances of complex **1** calculated with different basis sets and using the PBE1PBE functional (Calculated distance - experimental distance).

Basis set	Re1-Cl1	Re1-N3	Re1-N1	Re1-C1	Re1-C2	Re1-C3	Average deviation
LANL2DZ (Re) 6-31G+(d,p) (rest)	-0.003	-0.018	-0.021	-0.008	0.030	-0.011	0.015
LANL2DZ (Re) 6-311G+(d,p) (rest)	0.010	-0.021	-0.024	-0.009	0.031	-0.010	0.018
SDD (Re) 6-31G+(d,p) (rest)	0.003	-0.001	-0.003	0.004	0.041	0.001	0.009
SDD (Re) 6-311G+(d,p) (rest)	0.009	-0.002	-0.002	0.004	0.041	0.001	0.010
TZVPDD	-0.043	0.013	0.028	0.001	0.034	-0.006	0.021

Table S3. Frontier Molecular Orbital Compositions (%) in the Ground State for Complex **1** at the PBE1PBE Level

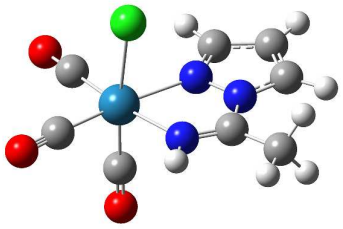

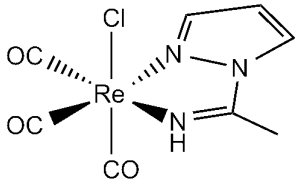

		Contribution (%)				
Orbital	Energy (eV):	Re:	Cl:	CO:	amidino:	main bond type
HOMO-4	-7.76	12.29	55.89	3.97	27.85	d(Re) + p(Cl) + π(amidino)
HOMO-3	-7.66	9.84	58.90	3.35	27.91	d(Re) + p(Cl) + π(amidino)
HOMO-2	-6.98	68.90	0.53	28.57	2.00	d(Re) + π(CO)
HOMO-1	-6.40	46.90	25.98	20.78	6.33	d(Re) + p(Cl) + π(CO)
HOMO	-6.32	47.08	25.77	22.84	4.32	d(Re) + p(Cl) + π(CO)
LUMO	-2.04	4.60	1.68	5.82	87.91	π*(amidino)
LUMO+1	-0.55	29.29	1.08	65.50	4.14	p(Re) + π*(CO)
LUMO+2	-0.31	27.97	2.90	61.25	7.89	p(Re) + π*(CO)

Table S4. Frontier Molecular Orbital Compositions (%) in the Ground State for Complex **2** at the PBE1PBE Level

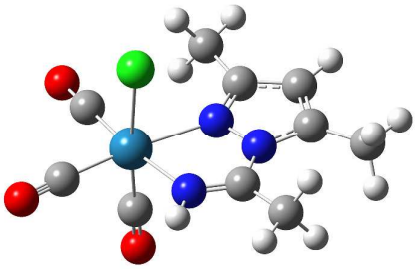

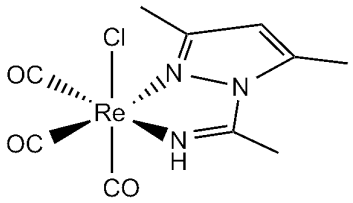

		Contribution (%)				
Orbital	Energy (eV):	Re:	Cl:	CO:	amidino:	main bond type
HOMO-4	-7.60	6.55	45.17	2.21	46.07	p(Cl) + π(amidino)
HOMO-3	-7.43	5.30	54.17	1.88	38.65	p(Cl) + π(amidino)
HOMO-2	-6.90	67.66	0.26	28.86	3.22	d(Re) + π(CO)
HOMO-1	-6.32	46.95	22.99	20.99	9.07	d(Re) + p(Cl) + π(CO)
HOMO	-6.26	47.34	24.58	22.89	5.20	d(Re) + p(Cl) + π(CO)
LUMO	-1.87	5.72	1.80	6.78	85.70	π*(amidino)
LUMO+1	-0.45	27.90	1.02	66.44	4.63	p(Re) + π*(CO)
LUMO+2	-0.25	26.72	2.72	60.20	10.36	p(Re) + π*(CO)

Table S5. Frontier Molecular Orbital Compositions (%) in the Ground State for Complex **3** at the PBE1PBE Level

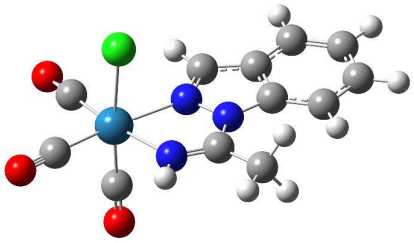

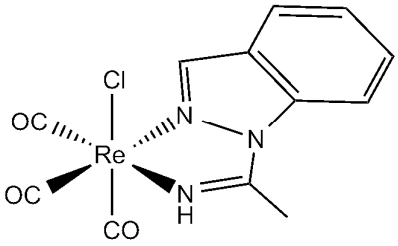

		Contribution (%)				
Orbital	Energy (eV):	Re:	Cl:	CO:	amidino:	main bond type
HOMO-4	-7.55	4.21	39.33	1.50	54.95	p(Cl) + π(amidino)
HOMO-3	-7.20	3.00	18.84	1.26	76.89	p(Cl) + π(amidino)
HOMO-2	-6.95	66.34	0.24	27.71	5.71	d(Re) + π(CO)
HOMO-1	-6.36	45.98	23.72	20.47	9.83	d(Re) + p(Cl) + π(CO)
HOMO	-6.29	46.34	24.92	22.16	6.58	d(Re) + p(Cl) + π(CO)
LUMO	-2.12	3.97	1.58	5.25	89.20	π*(amidino)
LUMO+1	-0.96	0.96	0.13	2.94	95.97	π*(amidino)
LUMO+2	-0.53	28.55	1.08	66.23	4.15	p(Re) + π*(CO)

Table S6. Frontier Molecular Orbital Compositions (%) in the Ground State for Complex **4** at the PBE1PBE Level

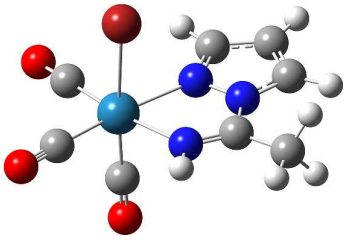

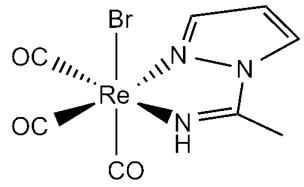

		Contribution (%)				
Orbital	Energy (eV):	Re:	Cl:	CO:	amidino:	main bond type
HOMO-4	-7.46	22.14	51.4	7.8	18.66	d(Re) + p(Br) + π(amidino)
HOMO-3	-7.35	17.76	54.04	6.07	22.13	d(Re) + p(Br) + π(amidino)
HOMO-2	-6.99	68.7	0.52	28.53	2.26	d(Re) + π(CO)
HOMO-1	-6.34	38.37	39.86	16.81	4.95	d(Re) + p(Br) + π(CO)
HOMO	-6.28	38.97	38.68	19.04	3.3	d(Re) + p(Br) + π(CO)
LUMO	-2.05	4.4	2.48	5.83	87.29	π*(amidino)
LUMO+1	-0.59	30.24	1.02	64.71	4.03	p(Re) + π*(CO)
LUMO+2	-0.36	27.72	4.52	59.84	7.92	p(Re) + π*(CO)

Table S7. Frontier Molecular Orbital Compositions (%) in the Ground State for Complex **5** at the PBE1PBE Level

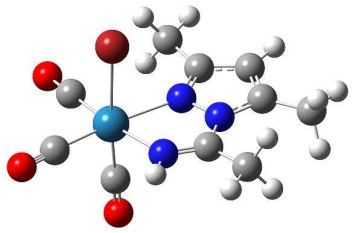

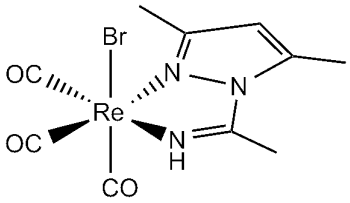

		Contribution (%)				
Orbital	Energy (eV):	Re:	Br:	CO:	amidino:	main bond type
HOMO-4	-7.34	16.88	48.95	6.14	28.02	p(Br) + π(amidino)
HOMO-3	-7.16	14.14	52.8	4.91	28.15	p(Br) + π(amidino)
HOMO-2	-6.91	64.93	1.81	27.89	5.37	d(Re) + π(CO)
HOMO-1	-6.27	39.56	35.73	17.49	7.22	d(Re) + p(Br) + π(CO)
HOMO	-6.22	39.73	36.95	19.31	4.01	d(Re) + p(Br) + π(CO)
LUMO	-1.87	5.45	2.7	6.81	85.03	π*(amidino)
LUMO+1	-0.49	28.91	0.98	65.55	4.56	p(Re) + π*(CO)
LUMO+2	-0.31	26.48	4.2	58.97	10.35	p(Re) + π*(CO)

Table S8. Frontier Molecular Orbital Compositions (%) in the Ground State for Complex **6** at the PBE1PBE Level

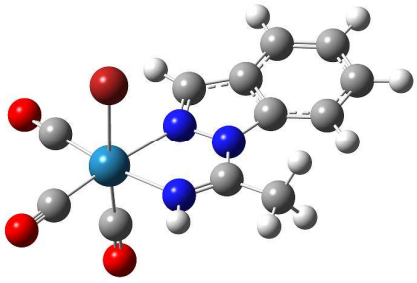

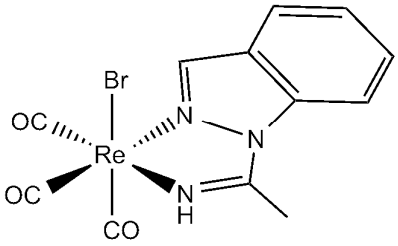

		Contribution (%)				
Orbital	Energy (eV):	Re:	Br:	CO:	amidino:	main bond type
HOMO-3	-7.09	14.84	30.61	5.64	48.91	d(Re) + p(Br) + π(amidino)
HOMO-2	-6.95	57.13	3.88	24.07	14.92	d(Re) + π(CO) + π(amidino)
HOMO-1	-6.32	38.54	36.9	17.02	7.54	d(Re) + p(Br) + π(CO)
HOMO	-6.26	38.75	37.42	18.6	5.22	d(Re) + p(Br) + π(CO)
LUMO	-2.13	3.84	2.31	5.27	88.58	π*(amidino)
LUMO+1	-0.96	0.98	0.21	3.07	95.74	π*(amidino)
LUMO+2	-0.57	29.53	1.02	65.4	4.06	p(Re) + π*(CO)
LUMO+3	-0.36	26.62	4.53	58.19	10.65	p(Re) + π*(CO)

Table S9. Frontier Molecular Orbital Compositions (%) in the Ground State for Complex **7** at the PBE1PBE Level

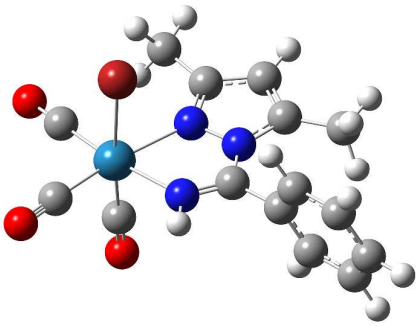

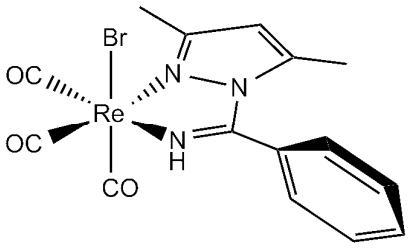

		Contribution (%)				
Orbital	Energy (eV):	Re:	Br:	CO:	amidino:	main bond type
HOMO-6	-7.82	0.9	1.62	0.45	97.03	π(amidino)
HOMO-5	-7.74	2.09	2.18	0.81	94.92	π(amidino)
HOMO-4	-7.33	15.39	45.45	5.81	33.35	d(Re) + p(Br) + π(amidino)
HOMO-3	-7.17	13.69	52.25	4.69	29.37	d(Re) + p(Br) + π(amidino)
HOMO-2	-6.93	65.15	1.67	27.82	5.37	d(Re) + π(CO)
HOMO-1	-6.29	39.26	36.34	17.26	7.14	d(Re) + p(Br) + π(CO)
HOMO	-6.24	39.52	36.86	19.34	4.28	d(Re) + p(Br) + π(CO)
LUMO	-2.01	4.72	2.49	6.06	86.74	π*(amidino)
LUMO+1	-0.84	5.83	0.46	7.79	85.92	π*(amidino)
LUMO+2	-0.53	1.5	0.24	3.06	95.19	π*(amidino)
LUMO+3	-0.47	26.04	1.34	61.75	10.88	p(Re) + π*(CO) + π*(amidino)

Table S10. Frontier Molecular Orbital Compositions (%) in the Ground State for Complex **8** at the PBE1PBE Level

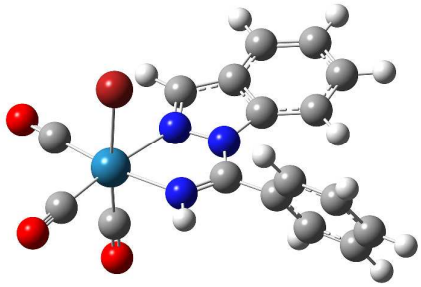

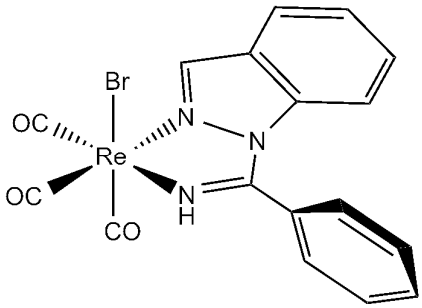

		Contribution (%)				
Orbital	Energy (eV):	Re:	Br:	CO:	amidino:	main bond type
HOMO-5	-7.55	14.5	20.43	5.43	59.65	d(Re) + p(Br) + π(amidino)
HOMO-4	-7.35	12.98	41.12	4.69	41.2	d(Re) + p(Br) + π(amidino)
HOMO-3	-7.07	15.01	30.52	5.73	48.74	d(Re) + p(Br) + π(amidino)
HOMO-2	-6.97	56.7	3.83	23.8	15.68	d(Re) + π(CO) + π(amidino)
HOMO-1	-6.32	38.19	36.44	16.86	8.52	d(Re) + p(Br) + π(CO)
HOMO	-6.28	38.57	38.32	18.65	4.46	d(Re) + p(Br) + π(CO)
LUMO	-2.19	3.8	2.32	5.2	88.69	π*(amidino)
LUMO+1	-1.24	0.48	0.04	1.85	97.63	π*(amidino)
LUMO+2	-0.71	13.12	0.61	23.48	62.79	p(Re) + π*(CO) + π*(amidino)

Table S11. Frontier Molecular Orbital Compositions (%) in the Ground State for Complex **9** at the PBE1PBE Level

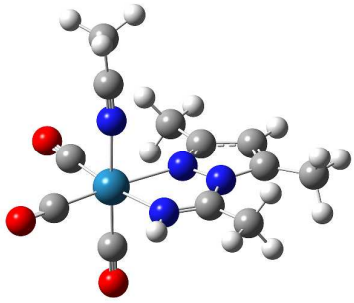

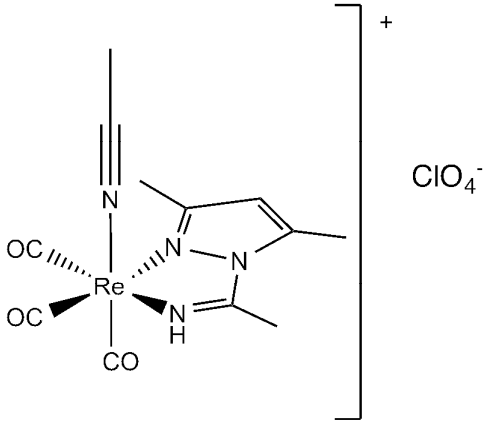

		Contribution (%)				
Orbital	Energy (eV):	Re:	MeCN:	CO:	amidino:	main bond type
HOMO-3	-8.39	6.21	1.44	2.11	90.25	π(amidino)
HOMO-2	-7.5	69.58	0	27.9	2.52	d(Re) + π(CO)
HOMO-1	-7.17	59.02	4.74	23.04	13.21	d(Re) + π(CO) + π(amidino)
HOMO	-7.11	54	4.09	21.28	20.63	d(Re) + π(CO) + π(amidino)
LUMO	-2.37	5.65	0.5	7.38	86.48	π*(amidino)
LUMO+1	-1.27	26.08	18.09	51.59	4.23	p(Re) + π*(CO) + π*(MeCN)
LUMO+2	-0.93	19.19	25.13	51.32	4.36	p(Re) + π*(CO) + π*(MeCN)

Table S12. Frontier Molecular Orbital Compositions (%) in the Ground State for Complex **10** at the PBE1PBE Level

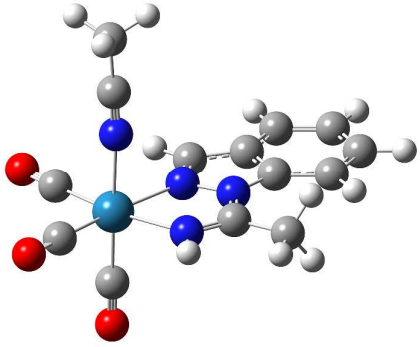

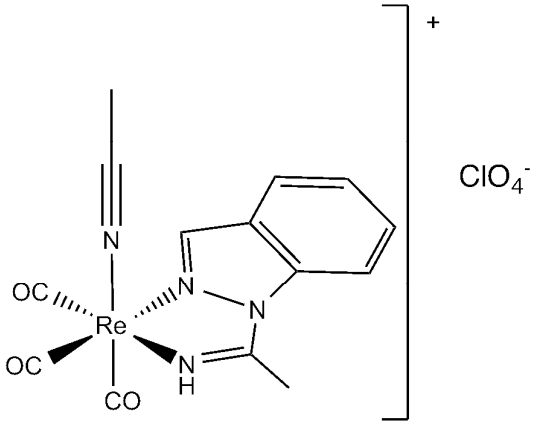

		Contribution (%)				
Orbital	Energy (eV):	Re:	MeCN:	CO:	amidino:	main bond type
HOMO-4	-8.38	10.66	2.24	3.39	83.71	d(Re) + π(amidino)
HOMO-3	-7.79	15.58	1.72	5.37	77.33	d(Re) + π(amidino)
HOMO-2	-7.54	68.75	0.01	27.13	4.12	d(Re) + π(CO)
HOMO-1	-7.21	57.16	4.63	22.67	15.54	d(Re) + π(CO) + π(amidino)
HOMO	-7.12	45.5	3.47	17.45	33.58	d(Re) + π(CO) + π(amidino)
LUMO	-2.6	4.23	0.45	5.9	89.42	π*(amidino)
LUMO+1	-1.36	10.51	6.9	20.56	62.03	π*(CO) + π*(amidino)
LUMO+2	-1.31	17.45	9.94	35.79	36.82	p(Re) + π*(CO) + π*(amidino)
LUMO+3	-0.97	19.45	23.74	51.89	4.91	p(Re) + π*(CO) + π*(MeCN)

Table S13. Frontier Molecular Orbital Compositions (%) in the Ground State for Complex **11** at the PBE1PBE Level

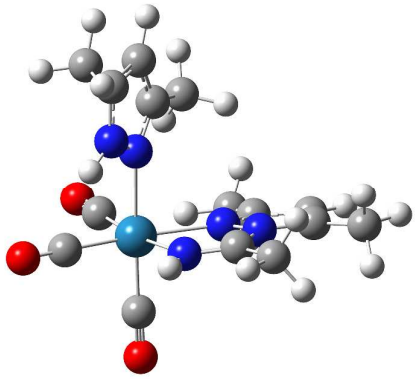

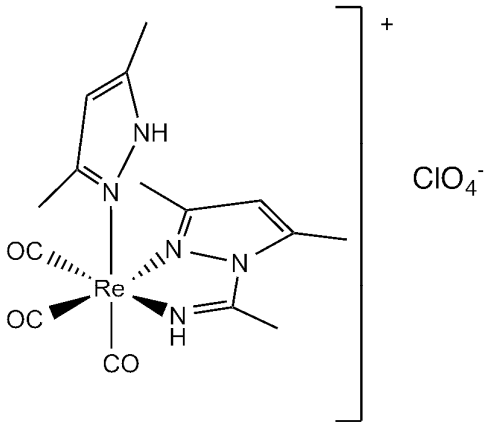

		Contribution (%)				
Orbital	Energy (eV):	Re:	dmpz:	CO:	amidino:	main bond type
HOMO-4	-8.10	6.49	74.87	2.42	16.22	π(dmpz) + π(amidino)
HOMO-3	-7.85	1.79	90.14	0.91	7.15	π(dmpz) + π(amidino)
HOMO-2	-7.52	68.78	0.84	28.62	1.76	d(Re) + π(CO)
HOMO-1	-7.20	59.52	0.98	24.36	15.14	d(Re) + π(CO) + π(amidino)
HOMO	-6.88	46.28	22.68	19.57	11.48	d(Re) + π(dmpz) + π(CO)
LUMO	-2.34	5.56	1.36	7.55	85.53	π*(amidino)
LUMO+1	-1.14	29.03	3.64	62.59	4.74	p(Re) + π*(CO)
LUMO+2	-0.82	18.50	17.13	56.85	7.52	p(Re) + π*(dmpz) + π*(CO)

Table S14. Frontier Molecular Orbital Compositions (%) in the Ground State for Complex **12** at the PBE1PBE Level

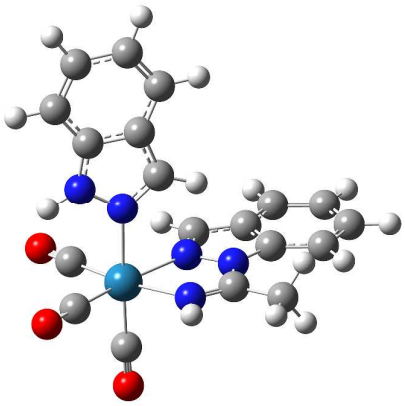

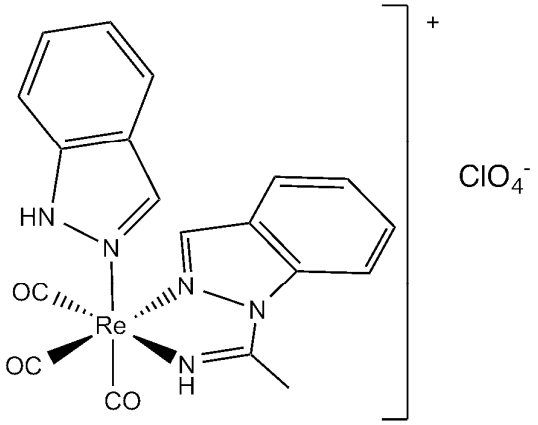

		Contribution (%)				
Orbital	Energy (eV):	Re:	indz:	CO:	amidino:	main bond type
HOMO-2	-7.22	46.02	2.75	17.87	33.35	d(Re) + π(CO) + π(amidino)
HOMO-1	-7.13	4.93	91	1.56	2.51	π(indazol)
HOMO	-7	42.34	30.35	18.64	8.67	d(Re) + π(CO) + π(indazol)
LUMO	-2.67	4.47	0.86	6.17	88.49	π*(amidino)
LUMO+1	-1.77	6.81	79.25	12.68	1.25	π*(indazol)
LUMO+2	-1.39	1.1	0.18	3.9	94.83	π*(amidino)

Table S15. Calculated Excited Energies, Dominant Orbital Excitations, and Oscillator Strength (*f*) from TD-DFT Calculations for Complex **1**

state	excitation	Coef.	E_{calc} (eV)	λ_{calc} (nm)	*f*	λ_{exp} (nm)	Character
S_1	HOMO → LUMO	0.70	3.21	386	0.0035		MLCT/LLCT/XLCT
S_2	HOMO-1 → LUMO	0.69	3.39	366	0.0964	360	MLCT/LLCT/XLCT
S_8	HOMO-4 → LUMO HOMO-3 → LUMO	0.64 0.27	4.76	261	0.1178	264	MLCT/XLCT/ILCT

Table S16. Calculated Excited Energies, Dominant Orbital Excitations, and Oscillator Strength (*f*) from TD-DFT Calculations for Complex **2**

state	excitation	Coef.	E_{calc} (eV)	λ_{calc} (nm)	*f*	λ_{exp} (nm)	Character
S_1	HOMO → LUMO	0.69	3.33	372	0.0033		MLCT/LLCT/XLCT
S_2	HOMO-1 → LUMO	0.69	3.49	356	0.1067	352	MLCT/LLCT/XLCT
S_7	HOMO-3 → LUMO	0.67	4.62	268	0.0855	261	XLCT/ILCT
S_8	HOMO-4 → LUMO	0.67	4.76	261	0.0850		XLCT/ILCT

Table S17. Calculated Excited Energies, Dominant Orbital Excitations, and Oscillator Strength (*f*) from TD-DFT Calculations for Complex **3**

state	excitation	Coef.	E_{calc} (eV)	λ_{calc} (nm)	*f*	λ_{exp} (nm)	Character
S_1	HOMO → LUMO	0.68	3.17	391	0.0031		MLCT/LLCT/XLCT
S_2	HOMO-1 → LUMO	0.67	3.34	371	0.1680	367	MLCT/LLCT/XLCT
S_4	HOMO-3 → LUMO	0.66	4.24	292	0.1652	304	XLCT/ILCT

Table S18. Calculated Excited Energies, Dominant Orbital Excitations, and Oscillator Strength (*f*) from TD-DFT Calculations for Complex **4**

state	excitation	Coef.	E_{calc} (eV)	λ_{calc} (nm)	*f*	λ_{exp} (nm)	Character
S_1	HOMO → LUMO	0.69	3.18	389	0.0023		MLCT/LLCT/XLCT
S_2	HOMO-1 → LUMO	0.69	3.32	373	0.0693	368	MLCT/LLCT/XLCT
S_7	HOMO-4 → LUMO HOMO-3 → LUMO	0.58 0.33	4.46	278	0.1262	267	MLCT/XLCT/ILCT

Table S19. Calculated Excited Energies, Dominant Orbital Excitations, and Oscillator Strength (*f*) from TD-DFT Calculations for Complex **5**

state	excitation	Coef.	E_{calc} (eV)	λ_{calc} (nm)	*f*	λ_{exp} (nm)	Character
S_1	HOMO → LUMO	0.69	3.32	374	0.0021		MLCT/LLCT/XLCT
S_2	HOMO-1 → LUMO	0.69	3.44	361	0.0795	356	MLCT/LLCT/XLCT
S_4	HOMO-3 → LUMO	0.63	4.35	285	0.0916	283	LLCT/ILCT
S_7	HOMO-4 → LUMO	0.64	4.48	277	0.0636		LLCT/ILCT
S_9	HOMO-1 → LUMO+2	0.59	4.85	255	0.0340	248	MLCT/LLCT/ILCT

Table S20. Calculated Excited Energies, Dominant Orbital Excitations, and Oscillator Strength (*f*) from TD-DFT Calculations for Complex **6**

state	excitation	Coef.	E_{calc} (eV)	λ_{calc} (nm)	*f*	λ_{exp} (nm)	Character
S_1	HOMO → LUMO	0.68	3.15	393	0.0025		MLCT/LLCT/XLCT
S_2	HOMO-1 → LUMO	0.67	3.29	377	0.1261	379	MLCT/LLCT/XLCT
S_4	HOMO-3 → LUMO HOMO-2 → LUMO	0.64 -0.22	4.13	300	0.2239	269	MLCT/XLCT/ILCT
S_{10}	HOMO → LUMO+1 HOMO → LUMO+3 HOMO-1 → LUMO+1	0.40 0.39 -0.30	4.49	276	0.0818	251	MLCT/LLCT/XLCT

Table S21. Calculated Excited Energies, Dominant Orbital Excitations, and Oscillator Strength (*f*) from TD-DFT Calculations for Complex **7**

state	excitation	Coef.	E_{calc} (eV)	λ_{calc} (nm)	*f*	λ_{exp} (nm)	Character
S_1	HOMO → LUMO	0.70	3.20	387	0.0019		MLCT/LLCT/XLCT
S_2	HOMO-1 → LUMO	0.70	3.33	372	0.0827		MLCT/LLCT/XLCT
S_4	HOMO-3 → LUMO	0.66	4.23	293	0.0996		MLCT/XLCT/ILCT
S_5	HOMO-4 → LUMO HOMO-1 → LUMO+3	0.54 0.27	4.34	286	0.0443		MLCT/LLCT/XLCT/ /ILCT
S_{10}	HOMO-6 → LUMO	0.66	4.74	261	0.0462		ILCT

Table S22. Calculated Excited Energies, Dominant Orbital Excitations, and Oscillator Strength (*f*) from TD-DFT Calculations for Complex **8**

state	excitation	Coef.	E_{calc} (eV)	λ_{calc} (nm)	*f*	λ_{exp} (nm)	Character
S_1	HOMO → LUMO	0.69	3.11	399	0.0026		MLCT/LLCT/XLCT
S_2	HOMO-1 → LUMO	0.69	3.24	383	0.1225	381	MLCT/LLCT/XLCT
S_4	HOMO-3 → LUMO	0.63	4.05	306	0.2035	310	MLCT/XLCT/ILCT
S_{10}	HOMO-5 → LUMO	0.65	4.32	287	0.1437	273	MLCT/XLCT/ILCT

Table S23. Calculated Excited Energies, Dominant Orbital Excitations, and Oscillator Strength (*f*) from TD-DFT Calculations for Complex **9**

state	excitation	Coef.	E_{calc} (eV)	λ_{calc} (nm)	*f*	λ_{exp} (nm)	Character
S_1	HOMO-1 → LUMO HOMO → LUMO	0.46 0.53	3.70	355	0.0133		MLCT/LLCT/ILCT
S_2	HOMO-1 → LUMO HOMO → LUMO	0.52 0.45	3.86	321	0.1784	324	MLCT/LLCT/ILCT
S_8	HOMO-2 → LUMO+2 HOMO → LUMO+2	0.40 0.40	4.97	250	0.0561	254	MLCT/LLCT/ILCT/ /LXCT
S_9	HOMO-3 → LUMO	0.67	5.12	242	0.1457	233	ILCT

Table S24. Calculated Excited Energies, Dominant Orbital Excitations, and Oscillator Strength (*f*) from TD-DFT Calculations for Complex **10**

state	excitation	Coef.	E_{calc} (eV)	λ_{calc} (nm)	*f*	λ_{exp} (nm)	Character
S_1	HOMO-1 → LUMO HOMO → LUMO	0.62 0.32	3.59	346	0.0078		MLCT/LLCT/ILCT
S_2	HOMO-1 → LUMO HOMO → LUMO	0.31 0.60	3.72	333	0.3427	340	MLCT/LLCT/ILCT
S_4	HOMO-3 → LUMO	0.67	4.33	286	0.0975		MLCT/ILCT
S_{10}	HOMO-4 → LUMO HOMO → LUMO+3	0.30 0.24	4.97	250	0.0670	246	MLCT/LLCT/ILCT/ /LXCT

Table S25. Calculated Excited Energies, Dominant Orbital Excitations, and Oscillator Strength (*f*) from TD-DFT Calculations for Complex **11**

state	excitation	Coef.	E_{calc} (eV)	λ_{calc} (nm)	*f*	λ_{exp} (nm)	Character
S_1	HOMO → LUMO	0.70	3.64	341	0.1508	346	MLCT/LLCT/XLCT
S_2	HOMO-1 → LUMO	0.70	3.77	329	0.0035		MLCT/LLCT/ILCT
S_8	HOMO-4 → LUMO HOMO-1 → LUMO+2	0.61 0.26	4.85	256	0.0713	260	XLCT/ILCT
S_9	HOMO → LUMO+2 HOMO-1 → LUMO+1	0.52 0.23	4.87	255	0.0727		MLCT/LLCT/LXCT

Table S26. Calculated Excited Energies, Dominant Orbital Excitations, and Oscillator Strength (*f*) from TD-DFT Calculations for Complex **12**

state	excitation	Coef.	E_{calc} (eV)	λ_{calc} (nm)	*f*	λ_{exp} (nm)	Character
S_1	HOMO → LUMO	0.68	3.38	367	0.0053		MLCT/LLCT/XLCT
S_2	HOMO-2 → LUMO	0.64	3.73	332	0.3409	359	MLCT/LLCT/ILCT
S_6	HOMO → LUMO+1	0.56	4.25	291	0.1982	282	MLCT/LXCT/ILCT

Table S27. Molecular orbital Compositions in the Excited States.

			Contribution (%)			
Complex	Orbital	Energy (eV):	Re:	"sixth" ligand:	CO:	amidino:
1	HOMO	-5.87	46.33	18.86	17.50	17.31
	LUMO	-2.37	5.66	2.43	8.96	82.95
2	HOMO	-5.72	44.18	17.81	18.08	19.93
	LUMO	-2.24	6.12	1.97	9.17	82.74
3	HOMO	-5.76	43.27	17.96	17.58	21.18
	LUMO	-2.40	5.03	2.06	8.16	84.75
4	HOMO	-5.85	42.77	25.28	16.02	15.93
	LUMO	-2.37	5.03	3.41	8.60	82.96
5	HOMO	-5.72	40.88	24.02	16.62	18.48
	LUMO	-2.24	5.49	2.86	8.88	82.77
6	HOMO	-5.76	39.84	24.25	16.03	19.88
	LUMO	-2.40	4.59	2.83	7.85	84.74
7	HOMO	-5.66	39.02	24.30	17.13	19.55
	LUMO	-2.65	5.55	1.69	6.35	86.41
8	HOMO	-5.77	39.68	22.66	16.11	21.56
	LUMO	-2.65	4.86	2.04	6.43	86.67
9	HOMO	-6.61	47.79	3.87	18.38	29.97
	LUMO	-2.78	5.19	0.61	7.48	86.72
10	HOMO	-6.75	41.81	3.31	15.71	39.17
	LUMO	-2.99	4.57	0.59	6.85	87.99
11	HOMO	-6.27	45.69	18.99	18.48	16.83
	LUMO	-3.07	4.44	1.92	5.38	88.26
12	HOMO	-6.60	42.39	13.71	16.14	27.76
	LUMO	-3.01	4.72	1.08	7.41	86.80

Table S28. Calculated Emission Energies and Dominant Orbital Emissions from TD-DFT Calculations.

Complex	state	Excitation	Coef.	E_{calc} (eV)	λ_{calc} (nm)	λ_{exp} (nm)	Character
1	T_1	HOMO → LUMO	0.69	1.88	659	570	^{3}MLCT/^{3}LLCT/^{3}XLCT
2	T_1	HOMO → LUMO	0.69	1.82	682	557	^{3}MLCT/^{3}LLCT/^{3}XLCT
3	T_1	HOMO → LUMO	0.68	1.84	672	559	^{3}MLCT/^{3}LLCT/^{3}XLCT
4	T_1	HOMO → LUMO	0.68	1.91	648	572	^{3}MLCT/^{3}LLCT/^{3}XLCT
5	T_1	HOMO → LUMO	0.68	1.88	661	564	^{3}MLCT/^{3}LLCT/^{3}XLCT
6	T_1	HOMO → LUMO	0.66	1.86	667	581	^{3}MLCT/^{3}LLCT/^{3}XLCT
7	T_1	HOMO → LUMO	0.68	1.48	840		^{3}MLCT/^{3}LLCT/^{3}XLCT
8	T_1	HOMO → LUMO	0.68	1.61	769	606	^{3}MLCT/^{3}LLCT/^{3}XLCT
9	T_1	HOMO → LUMO	0.67	2.07	599	524	^{3}MLCT/^{3}LLCT/^{3}ILCT
10	T_1	HOMO → LUMO	0.66	1.93	644	532	^{3}MLCT/^{3}LLCT/^{3}ILCT
11	T_1	HOMO → LUMO	0.67	1.77	699	536	^{3}MLCT/^{3}LLCT/^{3}XLCT
12	T_1	HOMO → LUMO	0.65	1.90	653	544	^{3}MLCT/^{3}LLCT/^{3}ILCT

Graphical Abstract

Luminescent Rhenium(I) Tricarbonyl Complexes with Pyrazolylamidino Ligands: Photophysical, Electrochemical, and Computational Studies

Patricia Gómez-Iglesias, Fabrice Guyon, Abderrahim Khatyr, Gilles Ulrich, Michael Knorr, Jose Miguel Martín-Alvarez, Daniel Miguel, and Fernando Villafañe*